compatible gallium selenide nanocrystals would therefore open the applications of these materials in bio-analytical chemistry. In a recent finding, it has been shown that the reaction between hot perchloric acid and gallium is a source of Ga^{3+} for synthesis of gallium selenide nanocrystals, which when functionalized with 3-mercaptopropionic acid acid gives rise to water soluble, bio-compatible nanocrystals (*Ndangili et al., 2011*).

2.3.2 Iridium selenide quantum dots

Platinum group metals (PGMs) are generally known for their similarities in physical and chemical properties. They are attracting attention in nanotechnology due to their catalytic activity, thermodynamic stability; with platinum and palladium on the fore front (*Lipshutz et al., 2012*; *Bond et al., 1968*). From these, PGM chalcogens, platinum group metal compounds that contain Seleniu d sometimes Oxygen (though oft are called oxides); due to the a chalcogenides in the electronic industry in multilayer ceramic c because of their semiconductor properties, they are being used resistance ohmic contacts. They also find applicability recording films in optical discs and lithographic films and light image receiving materials with silver halides (*Dey et al., 2004; Akhtar et al.,2010*). .

Now with the rise of nanotechnology it is inevitable for such compounds to be in the forefront in the nano-research community. In table 2, is a summary of a few findings on these compounds in nano-research:

Table 2 A summary of few findings on PGMs and PGM chalcogens in nano-research

Nanoparticle Composition	**Size**	**Application/ potential application**	**Reference**
$Pd_{20}Te_7$	12-15 nm	Catalysis	*Takahashi et al, 2011*

PdTe	5 nm	Catalysis	*Singh et al, 2012*
Rh	1-3 nm	Catalysis	*Almazo et al, 2005*
$RuSe_2$ nanotubes	6 nm wall thickness	Various	*Jiang et al., 2004*
$Pd_{17}Se_{15}$ nanotubes	6 nm wall thickness	Various	*Jiang et al., 2004*
Pt_3Te_4	4 nm	Catalysis	*Samal et al.,2010*
$Pd_{17}Se_{15}$	50 nm	Catalysis	*Akhtar et al.,2010*
$Ir_{50}Se_{50}$/C	Not reported due to agglomeration	Catalysis	*Liu et al., 2008*

2.3.3 3-Mercaptopropionic acid

Organothiols are mostly used to make self-assembled monolayers (SAMs), which are used to modify wetting properties of solid surfaces, to develop nano-devices for electronics and as corrosion preventative materials (*Boubour et al., 2000; Laibinis et al., 1992; Haag et al., 1999*) .They are now more scientifically attractive due to the ability of using their specific chemical groups in molecular recognition, protein adsorption on metals and templetes for crystallization (*Chailapakul et al., 1993; Ndangili et al., 2011*).

Organothiols have found their way into nanotechnology. During the synthesis of nanoparticles, organothiols such as mercaptopropionic acid, have been used as capping agents to prevent agglomeration of the nanoparticles as they form (*Ndangili et al., 2010*; *Moeno et al., 2011; Cookson et al., 2012).*

When suitably functionalized with amphiphilic bifunctional molecules such as mercapto carboxylic acids [HS- (CH2)n-COOH, n = 1–15], the small sizes of quantum dots can allow rapid transfer of electrons to the surface of the target particles, resulting to a higher charge detaching efficiency (*Liu et al., 2006; Idana et al., 2006*). The carboxylic group also offers a biocompatible surface since it can react favourably with amino groups of enzymes or antibodies without loss of enzyme or antibody activity. The short chained

capping agent mercaptopropionic acid (MPA), has been used for self-assembly on gold electrode and are associated with enhanced electrochemical signals of the quantum dots towards target analytes (*Giz et al., 1999; Li et al., 2009*).

2.4 Biosensors

Biosensors are small devices which employ bio-molecular recognition element as the basis for selective analysis. This electrochemical sensing device intimately couples a biological recognition element to an electrode transducer which converts the biological recognition event into a useful electrical signal (*Drummond et al., 2003*).

Thus, the major activities involved in any biosensor systems are analyte recognition, signal transduction and readout. As a result of their specificity, portability, speed and inexpensive nature, biosensors offer exciting opportunities for numerous applications. Glucose biosensor has brought a lot of revolution to the monitoring of sugar level in diabetics (*Cash et al., 2010*). Biosensors have also been used in the analysis of toxins, pollutants, diseases, genetically modified food, and in many other environmental, food, biomedical and explosive detection applications (Zhao et al., 2010; *Joseph et al., 2006)*. Though normally generalized, the bio recognition elements for biosensors are usually enzymes.

2.4.1 Cytochrome P450 3A4 (CYP3A4)

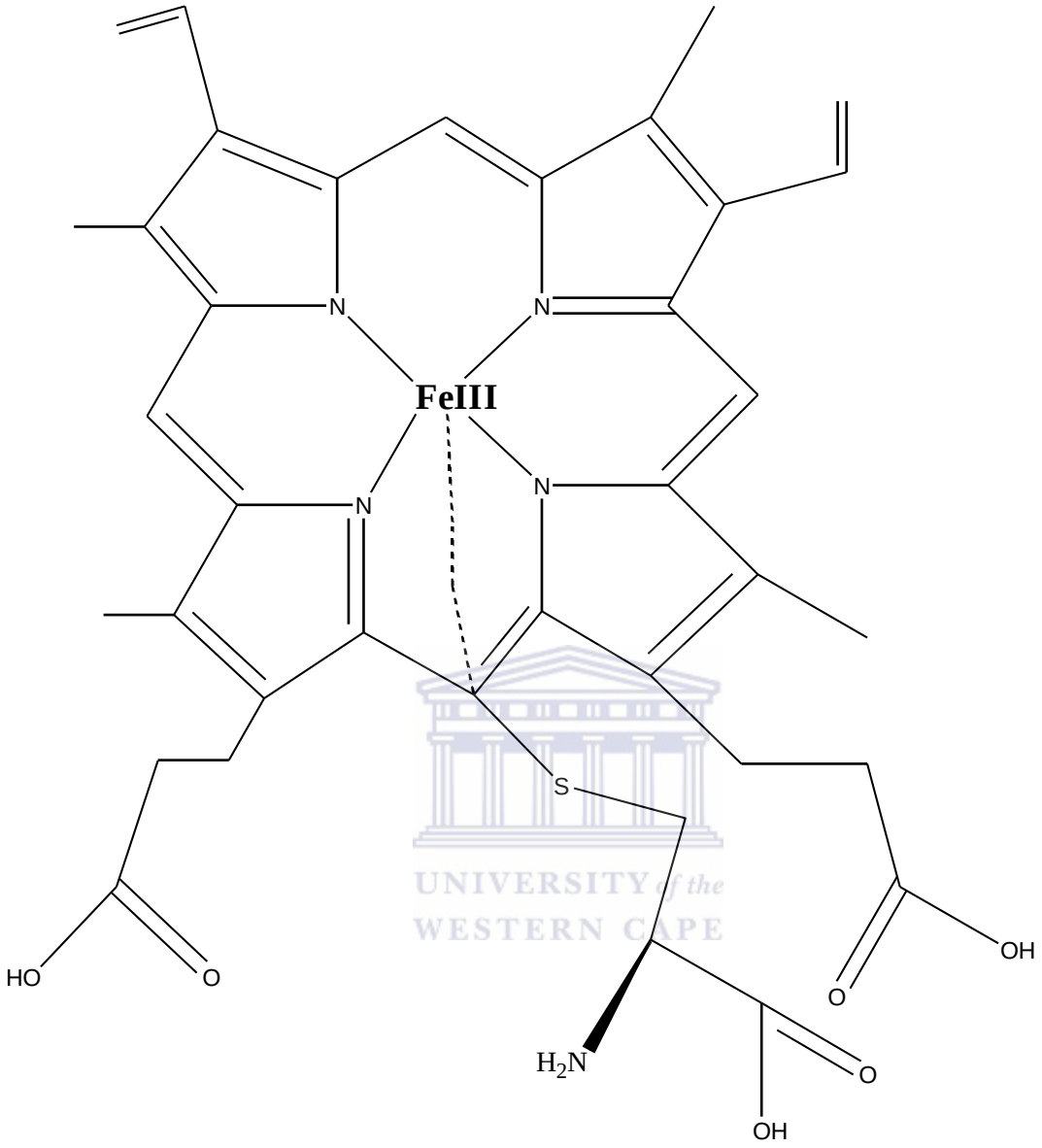

Figure 3 Cytochrome P450 3A4 (CYP3A4)

Cytochrome P450 iso-enzyme (CYP3A4) is the most catalytically versatile in the cytochrome P450 family, having the ability to catalyze the oxidative metabolism of various xenobiotic compounds which includes chlorophenols, pesticides, carcinogens, etc (Li et al., 1995; Bistolas et al., 2005). CYP3A4 oxidatively metabolizes 17alpha-ethinylestradiol / 17beta-estradiol to estrone as described in (Fig.4). The mono-oxygenation reaction of these compounds involves the reduction of the protein heme, from

Fe^{+3} to Fe^{+2}; and the hydrogenation of the substrate, 17alpha-ethinylestradiol / 17beta-estradiol (*Donato et al., 2003; Shumyantseva et al., 2005).*

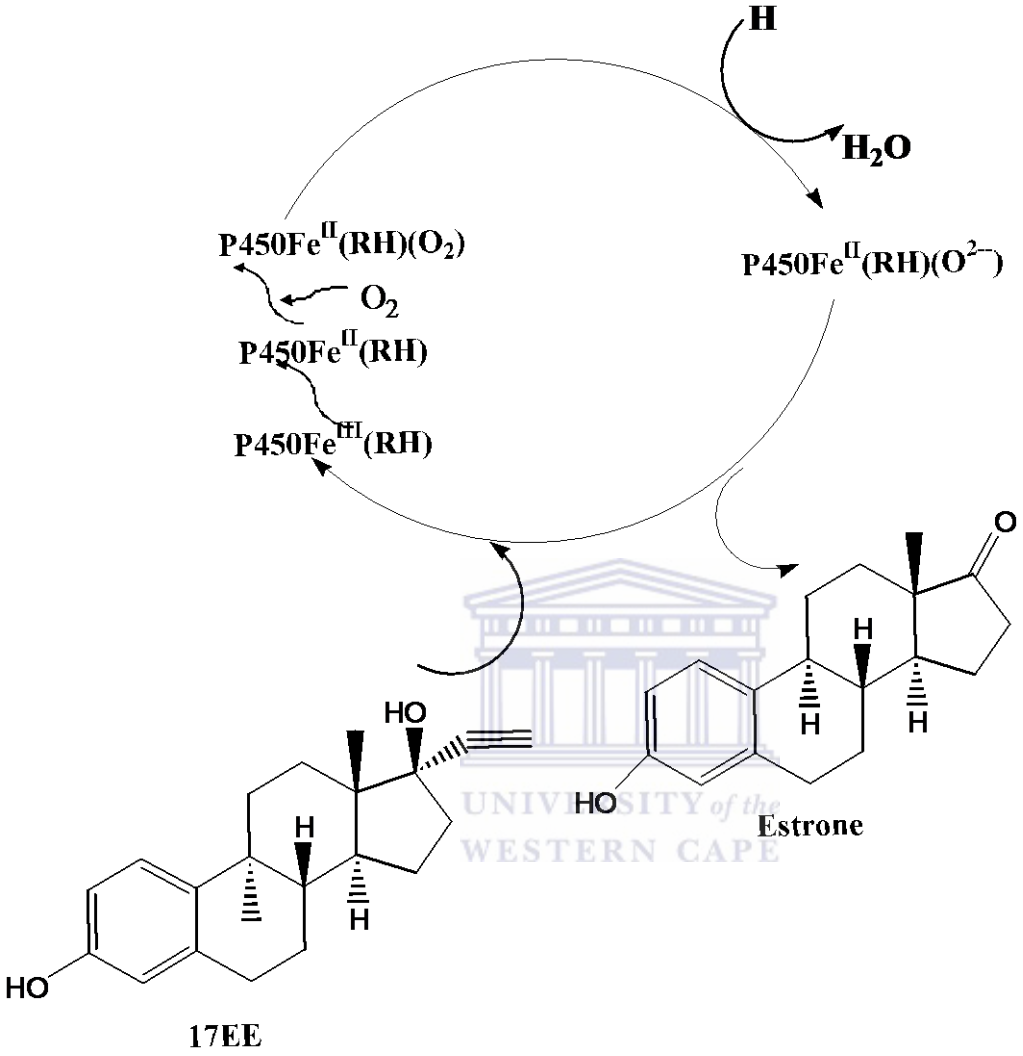

Figure 4 Oxidative metabolism of 17alpha-ethinylestradiol to estrone by CYP3A4

The active heme group is deeply embedded in the hydrophobic protein structure, such that it does not readily exchange electrons with metals or carbon electrode. Even though this cycle involves electronic transfer, but it is poor for electrochemical detection due to the entrapment of electrons in its hydrophobic structure. Thus for improved sensitivity, mediators have to be employed (*Hendricks et al., 2009*).

2.5 Imunosensors

Electrochemical sensors using antibodies or antigens as their bio-recognition element are called immunosensors. To understand the principle of immunosensing, we have to first understand the functional principle of immunoassays, as electrochemical sensors have been derived from them. An Immunoassay is a biochemical test used to measure concentrations of specific analytes in complex mixtures by making use of the fact that most analytes undergo specific immune reactions. These immune reactions involve an antibody-antigen binding pair whereby the analyte can be either an antibody/antigen. If the analyte is an antigen, an antibody will be used to assay the antigen, and vice versa (*Abad-Villar et al., 2002*)

Antibodies are gamma globulin proteins that are secreted as an immune response when antigens (bacteria, viruses, micro-organisms, drugs, etc) enter the bodies of vertebrates. These antibodies are highly specific as they will only form an antibody-antigen pair with specific antigens. They can be produced for a wide range of natural and man-made material, bio-molecules, and viruses. Their high specificity enables them to bind to specific targets even in complex systems where there might be different types of antigens (*Gong-Jun et al., 2009*).

Now, in electrochemical immunosensing two types of approaches are used namely labelled and label-free immunosensors, with the first being predominant. This is because in labelled immunosensors, the antibody/antigen is usually labelled with metals, enzymes, etc. The advantage of using metal labels is that they afford the possibility of using the sensitive stripping voltammetric techniques. Stripping techniques give the possibility of doing multiple analysis using six different metals for the detection of six different analytes. But the disadvantage of these labels is the usage of mercury electrodes which are

less desirable due to the toxicity of mercury. Hence now, enzymes are predominant as labels in electrochemical immunosensors (*Wijayawardhana et al., 2002*).

The enzyme-labelled electrochemical immunosensors afford signal amplification due to the catalytical activity of the enzymes. Usually the analyte species is the enzyme product. But this type of immunosensing is in most cases, an indirect approach for the detection of antigen.

On the other hand label free immunosensors offer a more simplistic approach which affords the direct quantification of a specific analyte. In table 3, are a few examples of label free immunosensors:

Table 3 Label free immunosensors

Type of immunosensor	**Analyte**	**Detection limit**	**Reference**
Label-free capacitative	E.Coli 0157:H7	2.2×10^{2} cfu /ml	D.Li et al., 2011
Label-free Amperometric immunosensor	E.Coli 0157:H7	250 cfu/ml	Y.Li et al., 2012
Label free capacitive Immunosensor	Microcystin-LR	1.0×10^{-14}M	Dawan et al., 2011
Label free capacitive Immunosensor	Benzylpenicilin	7.0×10^{-16}M	Dawan et al., 2011
Label free immunosensor	Anti-Biotin	30 ng/ ml	Liu et al., 2009

Chapter three

3.0 Experimental section

3.1 Experimental method for the construction of 3MPA-$IrSe_2$ based immunosensor and 3MPA-GaSe based biosensor

3.1.1 Instrumentation

Ultra violet-visible (UV-vis) absorption measurements were made on a Nicolet Evolution 100 UV–visible spectrometer (Thermo Electron, UK), using a quartz cuvette. All voltammetric and amperometric experiments were carried using a BAS100W integrated and automated electrochemical work station from Bio Analytical Systems (BAS), Lafayette, USA. All cyclic voltammograms were recorded with a computer interfaced to the BAS 100W electrochemical workstation. A 10 mL electrochemical cell with a conventional three electrode set up was used. The electrodes were: (1) Gold working electrode (A = 0.0201 cm^2) from BAS, modified with 3MPA-$IrSe_2$ quantum dots and anti-nodularin; (2) Gold working electrode (A = 0.0201 cm^2) from BAS modified with L-cysteine, Ga_2Se_3 -3MPA and CYP3A4 enzyme; (3) platinum wire, from Sigma Aldrich, acted as a counter electrode and (4) Ag/AgCl (3M KCl) from BAS was the reference electrode. Alumina micro polish and polishing pads were obtained from Buehler, IL, USA and were used for polishing the gold electrode before any modification.

Electrochemical impedance spectroscopy (EIS) measurements were recorded with Zahnner IM6 electrochemical work station from MeBtechnik at a bias potential of 0.222 V, amplitude of 5mV; recorded at a frequency range of 100 mHz to 100 Khz. A 10 mL electrochemical cell with a conventional three electrode set up was used. The electrodes were: (1) Gold working electrode (A = 0.0201 cm^2) from BAS, modified with 3MPA-

$IrSe_2$ quantum dots and anti-Nodularin antibody; (2) platinum wire, from Sigma Aldrich, acted as a counter.

3.1.2 Reagents

Analytical grade 3-mercaptopropionic acid ($HSCH_2CH_2CO_2H$) [3-MPA], sodium hydroxide, selenium powder, sodium borohydrate, hydrogen hexachloroiridate(IV) hydrate, gallium, perchloric acid, disodium hydrogen phosphate, sodium dihydrogen phosphate, potassium chloride ,1-ethyl-3-(3-dimethylaminopropyl) carbodiimide hydrochloride (EDC), N-hydroxysuccinimide (NHS), cyst1-ethyl-3-dimethylaminopropyl (L-cysteine), methanol, ethanol, bovine serum albumin (BSA), 17alpha-ethinylestradiol and 1 mg nodularin were all purchased from Sigma-Aldrich (Cape Town, South Africa). 0.10 M phosphate buffer saline (PBS) solution, pH 7.40, was prepared from disodium hydrogen phosphate, sodium dihydrogen phosphate and KCl.

Monoclonal nodularin antibody was purchased from Antibodies-online.Gmbh©, Germany; the production host is a mouse, IgG1 isotype. The aliquots were stored at -18 ˚C. All solutions were prepared using double distilled water. Genetically engineered cytochrome P450-3A4 (CYP3A4), purified from a full length human CYP3A4 cDNA clone, with a stock concentration of 37.74 µM was purchased from Merck South Africa while.

3.1.3 Synthesis of novel 3 mercaptopropionic acid capped iridium selenide quantum dots

NaHSe precursor was prepared by mixing 0.016 g of Se powder with 0.015 g of $NaBH_4$ in a round bottomed flask and adding de-ionized water to make 10 mL solution, resulting to 0.02 M and 0.04 M of Se and $NaBH_4$, respectively. The mixture was then stirred continuously at room temperature under nitrogen saturation for 25 min after which a dark yellow/ orange solution was formed. A 0.04 M of Ir^{IV} was prepared, and then 69.60 µL of

concentrated 3-mercaptopropionic acid (3MPA) added. The pH of the solution was adjusted to 12 using NaOH and saturated with N_2 for 30 min. Freshly prepared NaHSe was added drop wise into the nitrogen saturated Ir / 3MPA solution. After 10 min, a dark orange-brown solution was formed. The reaction was quenched by immediately placing the reaction flask in a freezer at -18 °C (*Shen et al., 2009; Ndangili et al., 2010*).

3.1.4 Fabrication of immunosensor

A gold electrode was polished with 1, 0.5, 0.03 μm alumina slurries on glassy polishing pads respectively (10 min on each pad), after which the electrode was ultrasonicated for about 15 min with distilled water and absolute ethanol to remove any possible absorbed alumina crystals on the electrode surface. Then it was electrochemically cleaned in 0.05 M sulphuric acid; which resulted to a clean gold electrode. The electrode was then immersed in 3MPA-$IrSe_2$ quantum dots for 12 h in the dark. Then the modified electrode was rinsed with ultra-pure water, to remove unbound quantum dots. The 3MPA-$IrSe_2$/Au electrode was immersed in (1:1) EDC and NHS to activate the QDs, and then rinsed lightly with ultra-pure water. 0.1 mg/mL anti-nodularin was drop coated onto the 3MPA-$IrSe_2$/Au electrode, and incubated for 4 h. To block undesired sites the immunosensor was then immersed into a solution of PBS ph 7.4 containing 1% BSA. This modification resulted into anti-nodularin/3MPA-$IrSe_2$/Au modified electrode which was then defined as the immunosensor. The immunosensor was then stored at 4 °C in 0.1 M PBS of pH 7.4 when not in use.

3.1.5 Immunosensor measurements

All the electrochemical measurements were carried out in 0.1 M PBS pH7.4 as the supporting electrolyte at room temperature, 25 °C. The 6.66 $x10^{-4}$ M nodularin stock solution was prepared using 99% methanol and stored at -18 °C. The substrate measurements were carried out under anaerobic condition.

3.1.6 Synthesis of 3-mercaptopropionic acid capped Ga_2Se_3 nanocrystals.

4.87 g of Ga metal was weighed into a round bottomed flask and 2 mL of concentrated $HClO_4$ was added. The mixture was refluxed under constant stirring for 4 h at 120 °C, after which a white precipitate of $Ga(ClO_4)_3.6H_2O$ was formed. 0.19 g of the gallium salt was dissolved in 10 mL of distilled water and 69.60 µL of concentrated 3-mercaptopropionic acid (3MPA) added. The pH of the solution was adjusted to 12 using NaOH and saturated with N_2 for 30 min. NaHSe precursor was prepared by mixing 0.016 g of Se powder with 0.015 g of $NaBH_4$ in a round bottomed flask and adding de-ionized water to make 10 mL solution, resulting to 0.02 M and 0.04 M of Se and $NaBH_4$, respectively. The mixture was then stirred continuously at room temperature under nitrogen saturation for 25 min after which a dark yellow solution was formed. Freshly prepared NaHSe was added drop wise into the nitrogen saturated $Ga(ClO_4)_3$/3MPA solution. After 10 min, a brown solution was formed and the reaction was quenched by immediately placing the reaction flask in a freezer at -18 °C (*Ndangili et al., 2011*)

3.1.7 Fabrication of 3MPA- Ga_2Se_3 based biosensor

A new Au electrode was polished with 1, 0.5, 0.03 µm alumina slurries on glassy polishing pads respectively (10 min on each pad) and ultrasonicated for about 15 min with distilled water and absolute ethanol to remove any possible absorbed alumina crystals on the electrode surface. The clean Au electrode was then immersed into a solution containing 0.02 M L-cysteine solution at room temperature for 24 h in the dark, to form self-assembled monolayer onto the gold electrode. The electrode was then rinsed carefully with distilled water to remove any unbound L-cysteine molecules. The L-cysteine modified electrode was then activated by immersing it into a solution containing 1:1 of EDC and NHS, for 20 min. Then the activated Au/L-cys modified electrode was immersed

into solution containing gallium selenide nanocrystals functionalized with mercaptopropionic acid (MPA), for 2 h to form Ga_2Se_3/L-cysteine modified gold electrode. The resulting nanocrystal modified gold electrode was allowed to dry for some time under nitrogen gas. 3 μL of a 4 μM CYP3A4 enzyme solution was then drop coated onto the 3MPA-Ga_2Se_3 modified electrode surface and allowed to imobilize for 3 h at 2 °C. This modification resulted into CYP3A4/ 3MPA-Ga_2Se_3 /L-cysteine/Au modified electrode which was then defined as the biosensor. The biosensor was then stored at 2 °C in 0.1 M PBS of pH 7.4 when not in use (*Nxusani et al., 2012*).

3.1.8 Biosensor measurements

All the electrochemical measurements were carried out in 0.1 M PBS pH7.4 as the supporting electrolyte at room temperature, 25^0C. The 0.01 mM, 0.001 mM, 0.0001 mM, 0.00001mM 17alpha-ethinylestradiol solutions were prepared using 0.1 M PBS solution. The substrate measurements were carried out under aerobic conditions.

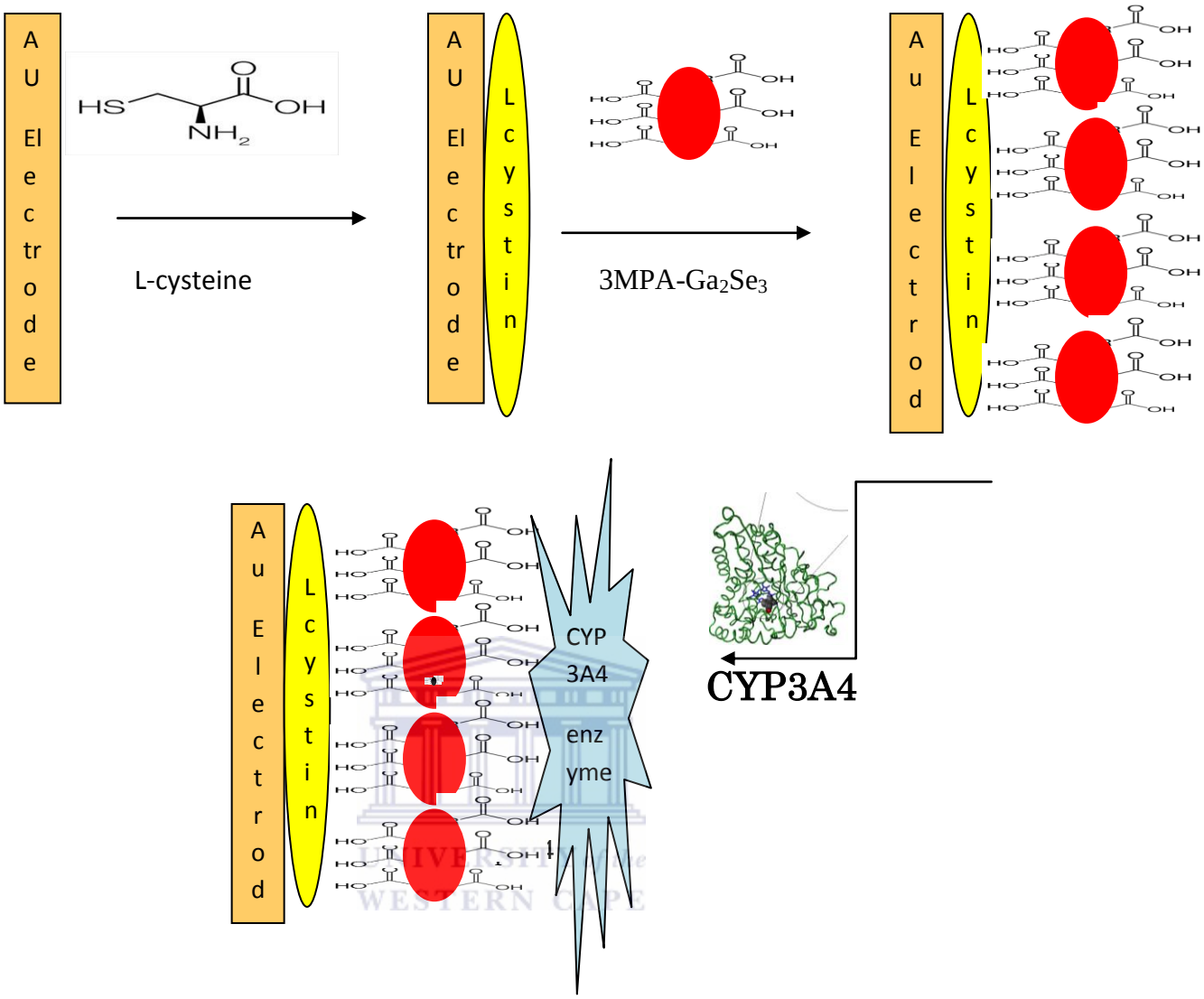

Scheme 1. Schematic representation of of 3MPA-GaSe based biosensor fabrication process

(Nxusani et al., 2012)

Chapter four

4. Results and Discussion

4A.1 Characterisation of 3-mercaptopropionic acid capped iridium selenide quantum dots

4A.1.1 Optical properties of the 3MPA-$IrSe_2$ quantum dots

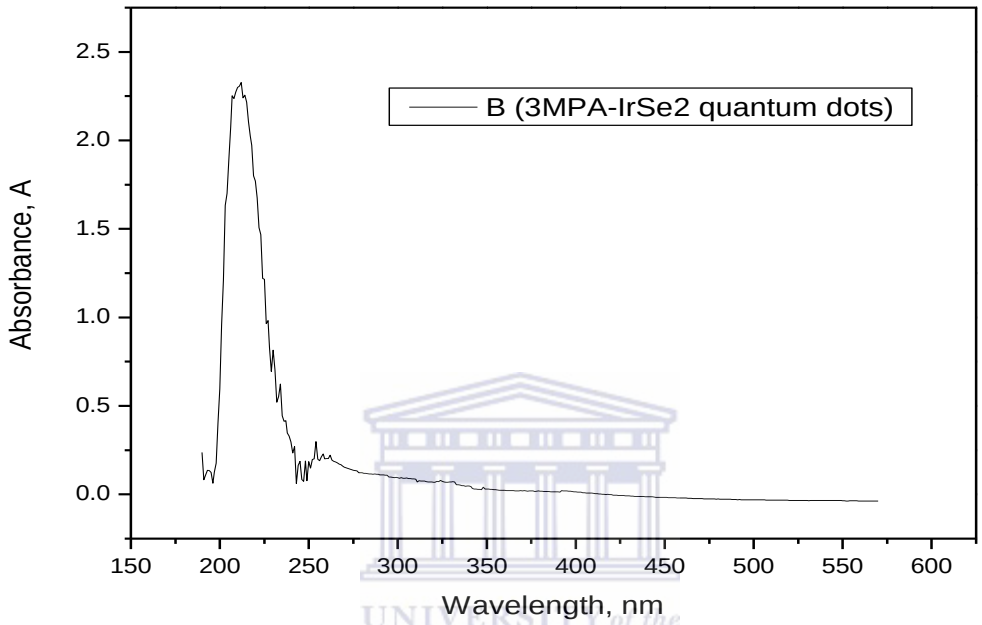

Figure 5 UV-vis spectrum of 3MPA-$IrSe_2$ quantum dots

The nature of the interaction between the valence and conduction band and the size of the band gap, determine the optical properties of quantum dots. The UV-vis spectroscopy of the 3MPA-iridium selenide quantum dots shown in Fig.5, shows a sharp absorption maxima at 210 nm. This indicates a formation of quantum dots that are homogeneous in their size distribution. From this the band gap energy of the quantum dots was found to be 5.6 eV equivalent to 9.459 x 10^{-19} J, calculated using the following formula:

$$E = hc/\lambda$$

Where E is the band gap energy, h is Planck's constant, c is the speed of light, λ is the experimental optical absorption wavelength.

The optical band gap energy of bulk Iridium Selenide is approximately 1.0 eV (*Dey et al., 2004; Strehlow et al., 1973*) meaning that the quantum dots formed had a six fold increase of band gap energy. This phenomena confirms the formation of very small sized particles, since the Effective mass approximation (EMA) first described by Louis Brus, states that as semiconductor materials decrease in size their band gap energies increase. Also for semiconductors with sizes smaller than 10 nm, the quantum size effect (QSE) becomes observable which predicts the widening of the band gap with decreasing size.

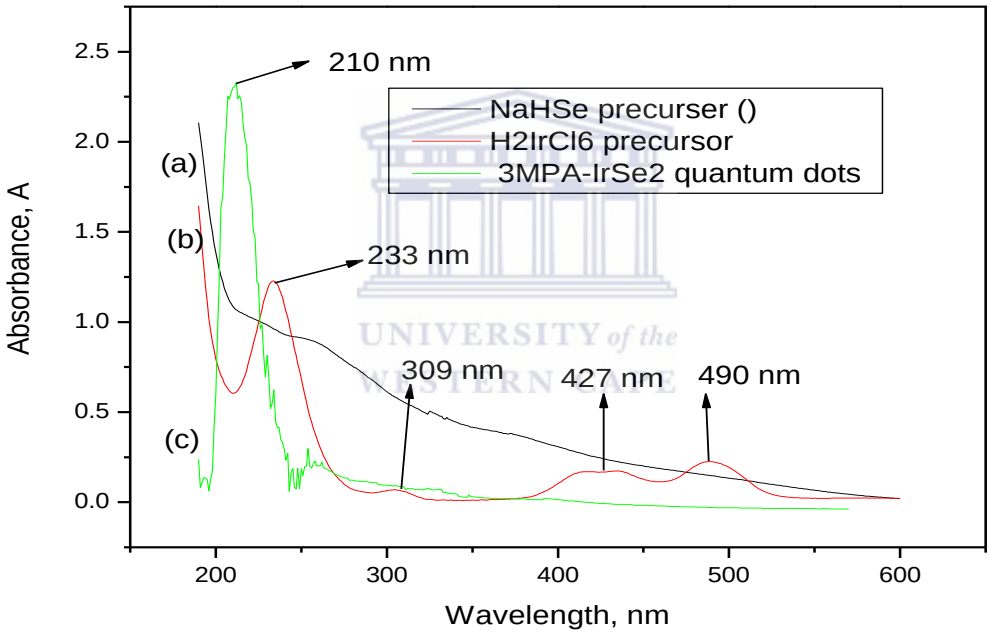

Figure 6 Uv spectrum of (a) NaHSe precursor, (b) 3MPA-IrSe quantum dots and (c) H_2IrCl_6.xH20 metal precursor

In Fig.6, the Uv-vis spectrum of the quantum dots and precursors is shown, where the absorption wavelength of the NaHSe precursor has a very broad absorption maxima at about 215-350 nm, and the absorption wavelengths of the H_2IrCl_6 are between 410 -494 nm. The absorption wavelength of the 3MPA-$IrSe_2$ quantum dots is very distinct and is blue-shifted below the region where the absorption wavelengths for both precursors are found.

4A.1.2 Microscopy of 3MPA-$IrSe_2$ quantum dot

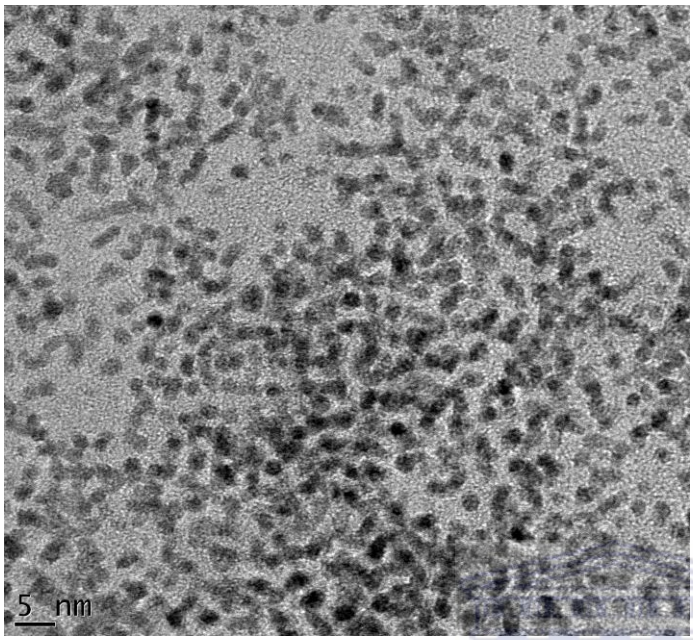

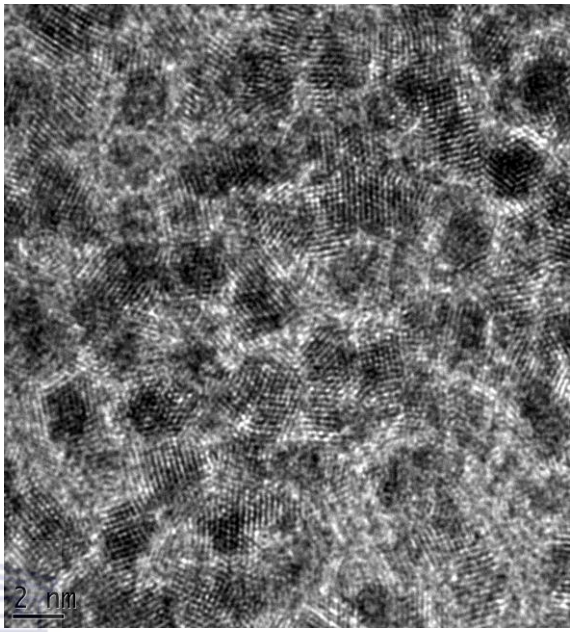

Figure 7 HRTEM micrographs of 3MPA-$IrSe_2$ quantum dots , 5 nm scale view (left); and 2 nm scale view (right)

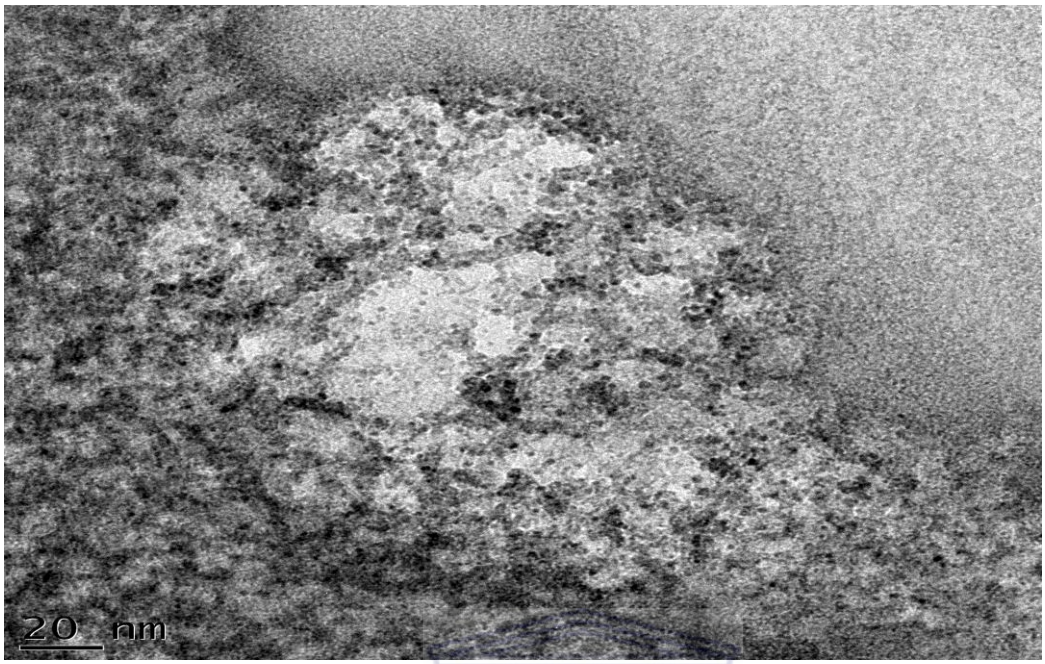

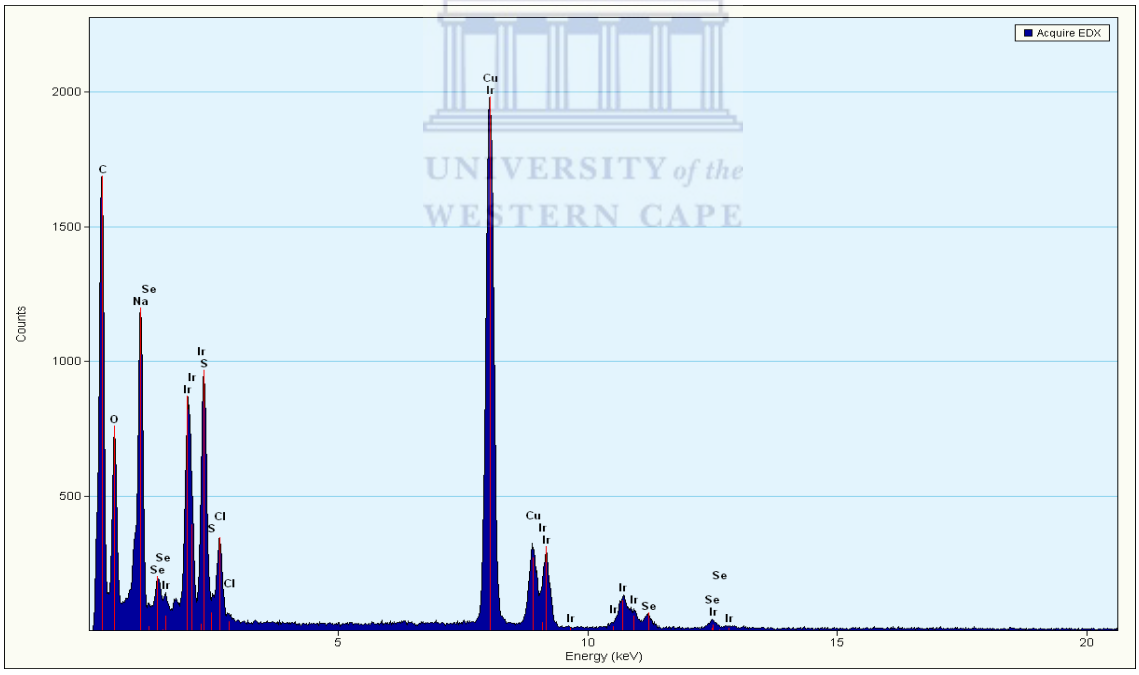

Figure 8 Energy dispersive X-Ray (EDX) spectrum of 3MPA-$IrSe_2$ quantum dots (below), taken from a highly populated region indicated on the (Above).

The High resolution transmission electron micrographs of the 3MPA-$IrSe_2$ quantum dots Fig 7, show the formation of quantum dots with an average diameter of 3 nm. This confirms the optical properties derived from the UV-vis absorption spectrum i.e the

formation of very small particles. In Fig 8, the chemical composition of the quantum dots was studied using energy dispersive x-ray spectroscopy and it revealed that the most abundant elements are Ir and Se.

4A.1.3 Electrochemistry of 3MPA-$IrSe_2$ quantum dots

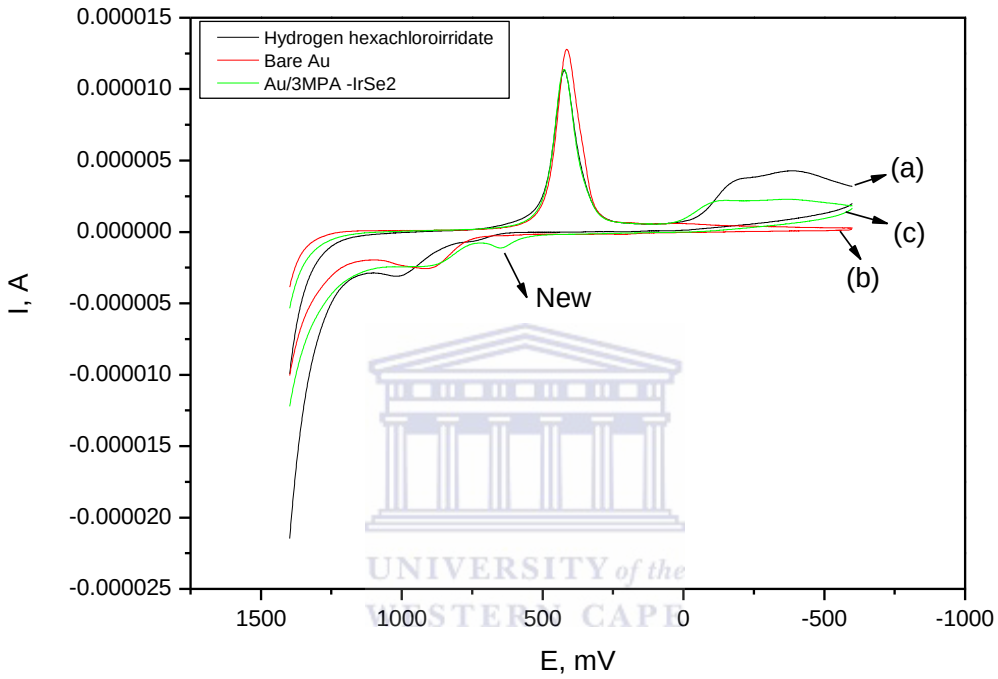

Figure 9 Cyclic voltammograms of (a) Au/ $H_2IrCl_6.xH_2O$ metal precursor, (b) bare Au ,and (c) Au/ 3MPA-$IrSe_2$ quantum dots in Phosphate Buffer pH 7.41 at 30 mV/s

Using cyclic voltammetry the electrochemical properties of 3MPA-$IrSe_2$ quantum dots as shown in Fig.9, were studied. The voltammograms revealed that the $H_2IrCl_6.xH_2O$ metal precursor has a reduction peak at about -182 mV which is absent on the bare Au, which is due to the reduction of Ir. Now notice that this reduction peak appears at -107 mV for the quantum dots and have a lower peak current. This is due to electron-confinement in three dimensions, which intern enhances the electrochemical reaction. The quantum dots lower

the activation energy for the reaction, causing a shift toward lower reductive potential, denoting a faster reduction reaction.

Also an oxidation peak at +641 mV was observed in the quantum dots which was absent in the bare Au and $H_2IrCl_6.xH_2O$ metal precursor. This is attributed to the oxidation of selenium as shown in Fig. 10. A shift towards lower oxidative potential is observed, indicative of the lowered activation energy for the oxidation reaction.

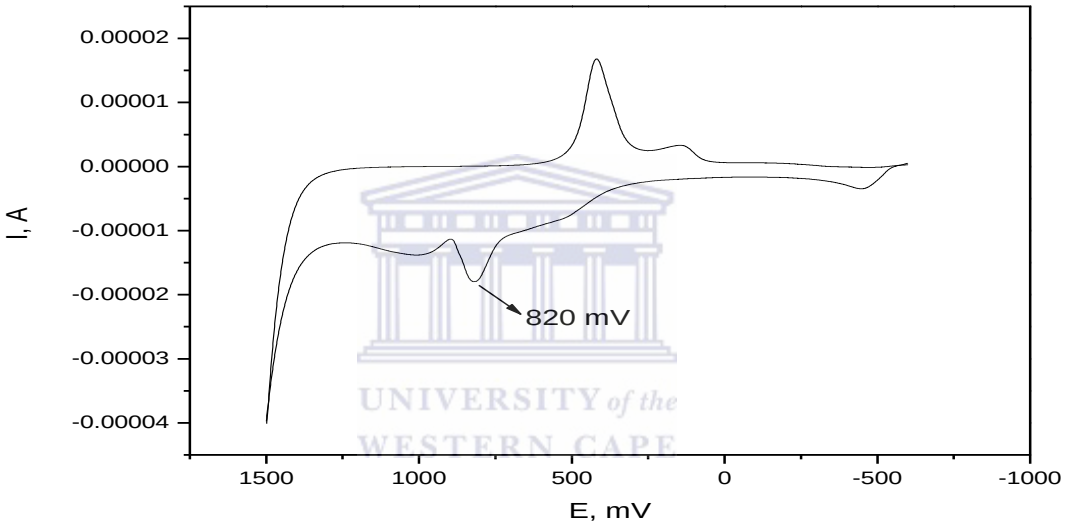

Figure 10 Cyclic voltamogram of Au/NaHSe precursor in Phosphate Buffer pH 7.41 at 30 mV/s

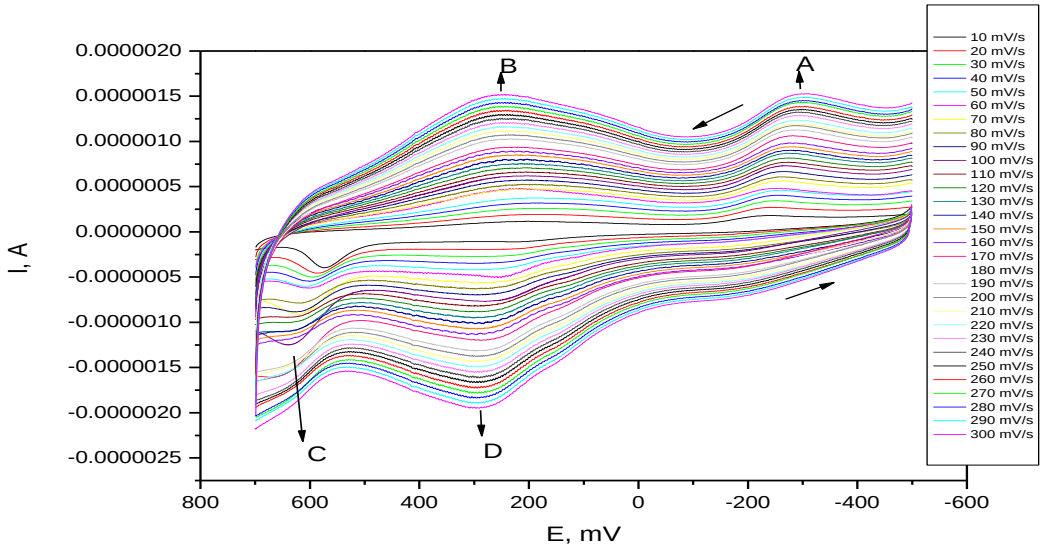

Figure 11 Multi-scan rate study of 3MPA-$IrSe_2$ quantum dots using cyclic voltammetry, in PBS pH 7.4

A multi-scan rate study of the 3MPA-$IrSe_2$ quantum dots on a gold electrode was performed as indicated in Fig.11, to investigate the electrochemistry of the quantum dots, scanning between -600 mV and 800 mV, scan rate 10-300 mV/s and in PBS pH7.4 The forward scan revealed two peaks (A and B) and on the reverse scan two peaks (C and D). The peak potential of A was found to be independent of the scan rate, with C having a non linear change in peak potential with scan rate.

Peak A is due to the reduction of Ir, B arises from the gold electrode similar to Fig 9; C and D are due to the oxidation of selenium similar to Fig. 10.The nonlinearity of C is due to the anodic stripping of Se, arising from the electro-oxidation of Se related surface states (*Ndangili et al, 2011*).

A close study of the reduction peak A was performed by constructing a plot of i_p (Peak current) versus v (scan rate), as illustrated in Fig 12. The peak current increased linearly (R=0.99) with scan rate, indicating the electrochemistry of surface confined quantum dots.

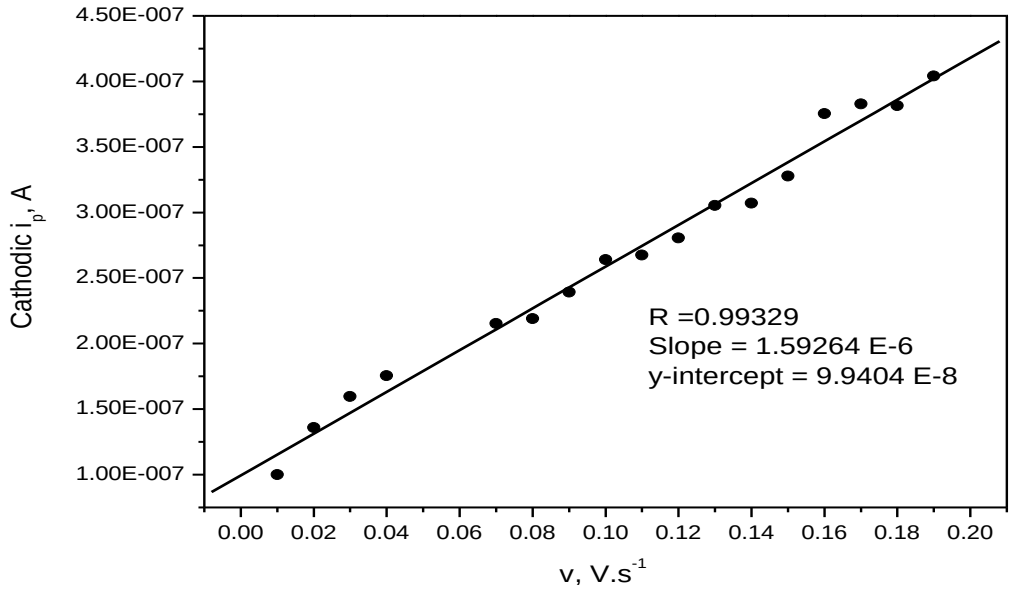

Figure 12 Cathodic plot (Peak A) of peak current versus scan rate

To estimate the no of electrons involved in this reduction of Ir (Peak A), the two equations:

$$I_p = \omega n^2 F^2 A \Gamma v / 4RT \qquad \text{(I) Laviron's equation}$$

$$Q = nFA\Gamma \qquad \text{(III)}$$

were re-expressed (*Zhang et al., 2005*) to the following equation:

$$i_p = nFQv / 4RT \qquad \text{(III)}$$

Where ω is the angular frequency, n the no of electrons, F is Faraday's constant (96 584 C/ mol), A is the electrode area, Γ is the surface concentration (mol/ cm^2), *v* is the scan rate, R is the gas constant (8.314 J/ mol. K), T is the temperature (298 K), Q is the quantity of charge calculated from the reduction peak area of the voltammograms. From the slope of plot i_p versus *v* Fig. 12, with the use of equation (III) the reduction process of the Ir of the quantum dots is estimated to involve four electrons. This indicates the

reduction of Ir^{IV} to Ir, which is usually a four electron process (*Pourbaix et al., 1959*). Thus, the oxidation state of the iridium metal of the quantum dots is Ir^{IV}.

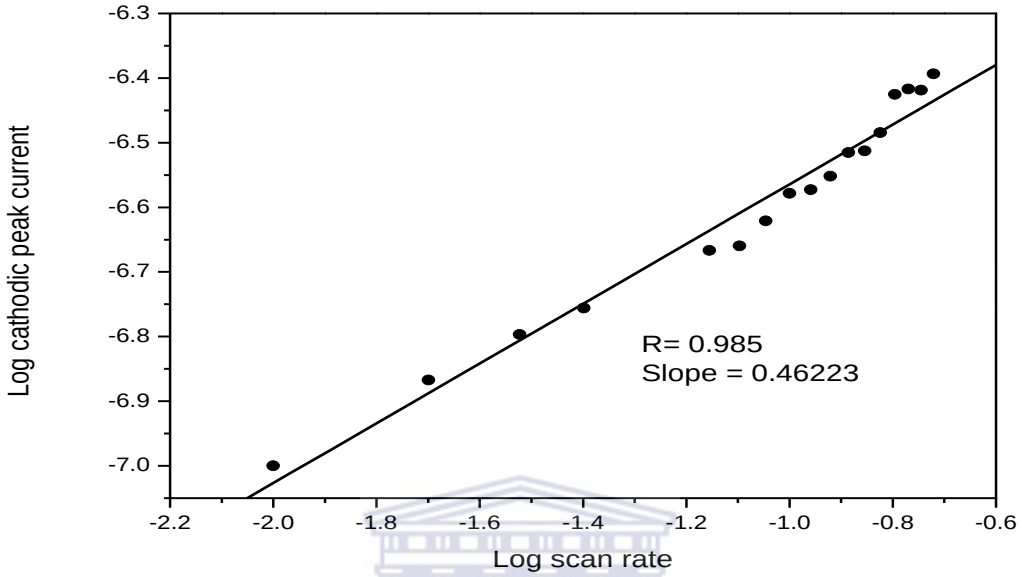

Figure 13 Log cathodic peak current versus log scan rate for peak A

The slope of plot Log cathodic peak current versus log scan rate as shown in Fig. 13, is 0.46, which indicates a diffusion controlled process (Ndangili et al., 2011). This means that the reduction of Ir occurs rapidly, thus denoting a fast redox reaction, which can also be observed from the increase of peak current with increasing scan rate (Fig. 11).

Furthermore, the reduction peak A was studied using chronocoulometry, as shown in Fig.14. In the Anson's plot (using BAS 100), at a pulse width of 20 msec the plots showed a wider peak separation. Using Anson's equation:

$$Q = 2nFCD^{1/2}t^{1/2} / \Pi^{1/2} \qquad \text{(IV)}$$

Where n is the no of electrons, F is the Faraday's constant, D is the diffusion coeffiecient, t is the time, C concentration (0.1 mol/dm^3 of PBS), and Π; from the slope of the Anson's plot (forward) scan, the diffusion coefficient is calculated to be 6.215 x 10^{-26} m^2/s.

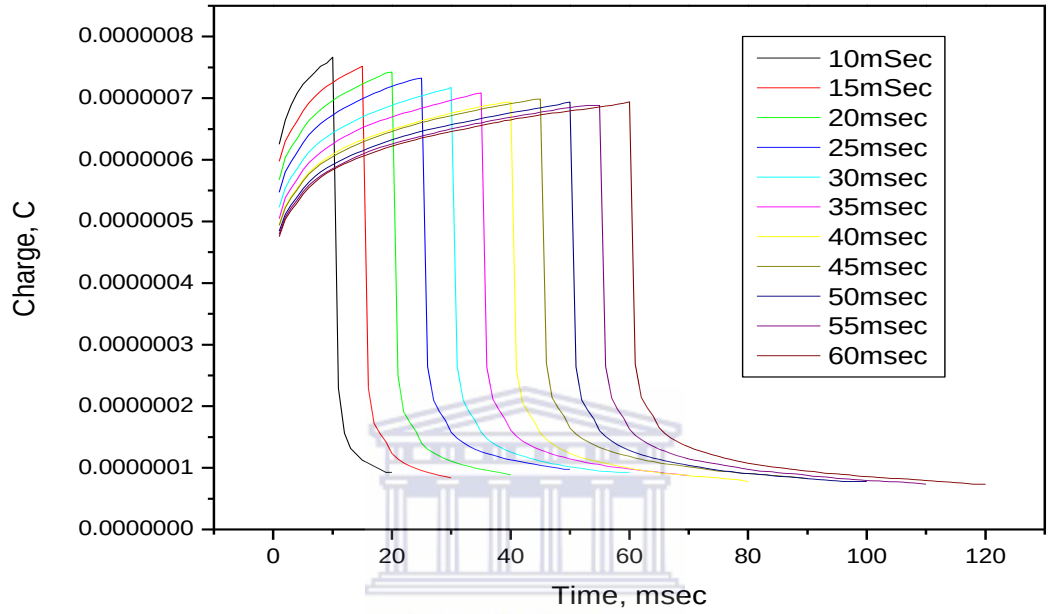

Figure 14 Chronocoulometry plot of the reduction (peak A) of 3MPA-$IrSe_2$

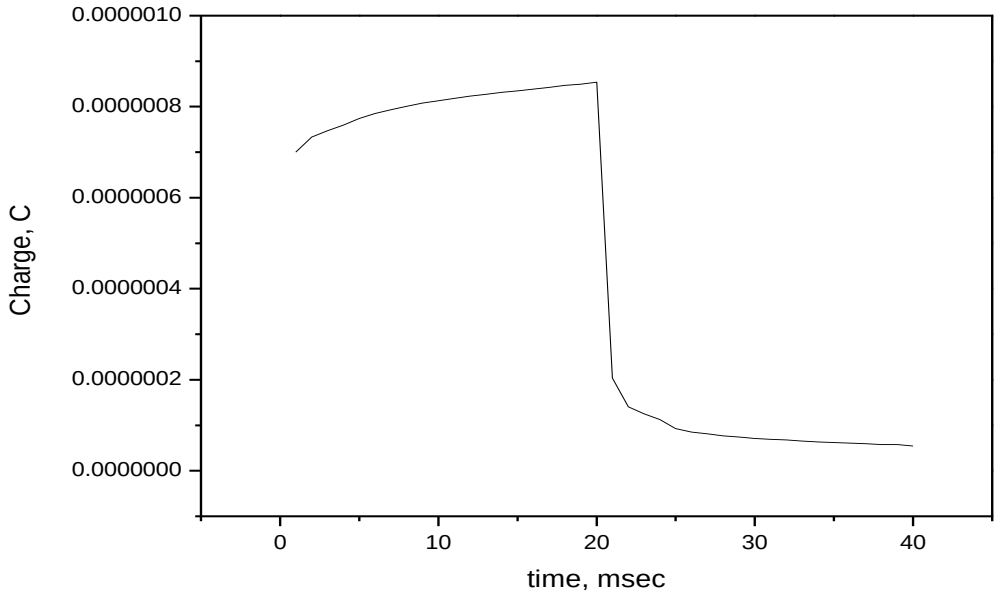

Figure 15 Chronocoulometry plot at pulse with of 20 msec

From the separation of charges at the y-intercept, the surface concentration of the adsorb species is given by:

$$Q_{ads} = nFA\Gamma \qquad (V)$$

Where Q_{ads} is the charge due to the electrolysis of the adsorbed species, and Γ is the surface concentration of the adsorb species. The charge due to the electrolysis of the 3MPA-$IrSe_2$ quantum dots is 4.0 nC and the surface concentration is 5.15 x 10-^{13} mol/cm^2.

4A.2. Characterisation using electrochemical impedance spectroscopy

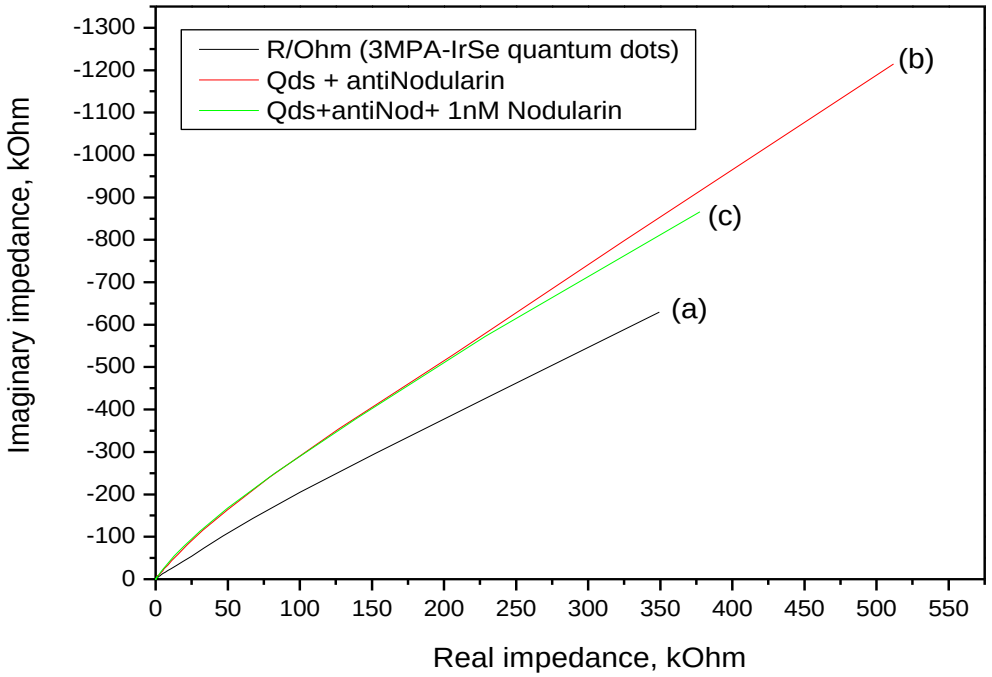

Figure 16 Nyquist plots of a) Au/3MPA-IrSe quantum dots, b) Au/3MPA-IrSe qds/antiNodularin, c) Au/3MPA-IrSe quantum dots/ antiNodularin+ 1nM Nodularin,; performed in 0.1 M PBS buffer pH7.4.

The electrochemical impedance spectroscopy was used to characterize the fabrication of 3MPA-$IrSe_2$ quantum dots based immunosensor as described in Fig.16.

Table 4 Circuit parameters for the fabrication of 3MPA-$IrSe_2$ quantum dots immunosensor

Electrode system	**Equivalent circuit A**		**Equivalent circuit B**	
	Zw	**% Error**	**Rct**	**% Error**
(a) 3MPA-$IrSe_2$ quantum dots	0.566 $\Omega.s^{-1/2}$	2.07	541.31 kΩ	10.99
(b) Au/3MPA-IrSe qds/antiNodularin	0.533 $\Omega.s^{-1/2}$	5.06	1090.90 kΩ	10.48

A)

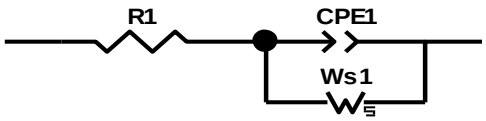

B)

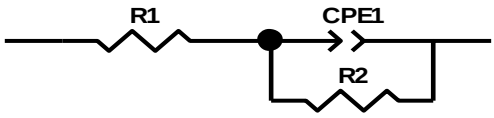

C)

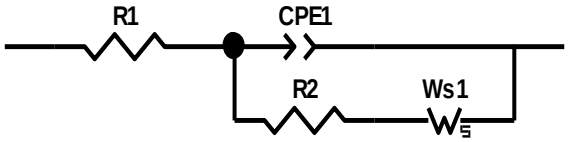

Figure 17 Equivalent circuits describing electrode modification process, fig 16

The Nyquist plots for the fabrication of the immunosensor, shown in Fig.16 are described by Equivalent circuit A-C, as shown in Fig.17. It was observed that for the 3MPA-$IrSe_2$ quantum dots, the circuit that best describes the process is circuit A, where R1 is the solution resistance, Ws1 is the Warburg impedance, CPE1 is the constant phase element. The Warburg impedance (Zw) percentage error shown in table 4 for the quantum dots when using equivalent circuit A, is lower than that of the quantum dots + antibody; and the charge transfer resistance (Rct) percentage error is higher than that value obtained from the circuit B. This indicates that the electrochemical process for the quantum dots is controlled by Zw. It therefore denotes that the electrochemical impedance for the quantum dots is a diffusion control process, meaning it is a fast electrode reaction; further complementing the results obtained from multi-scan rate analysis using cyclic voltammetry. Comparing the Zw and Rct, we obtain a trend described in Fig. 18-19.

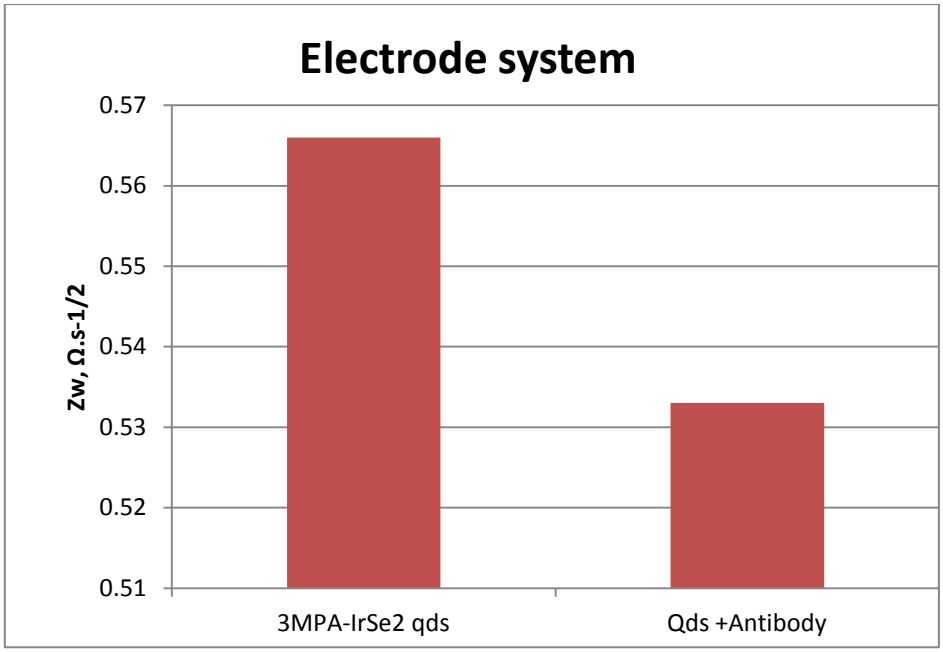

Figure 18 Chart showing the decrease in Warburg Impedance after antibody immobilisation

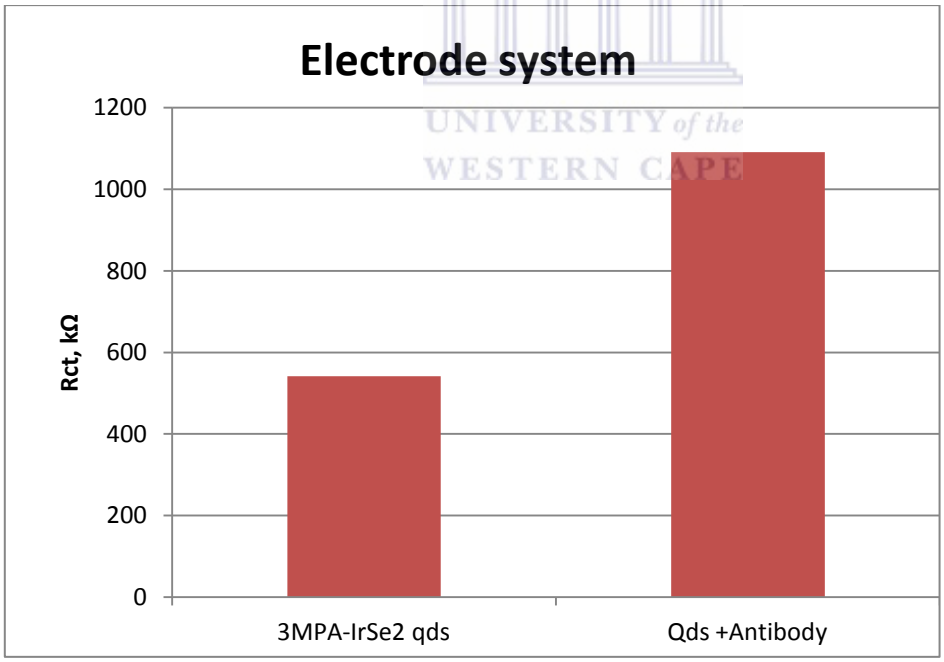

Figure 19 Chart showing the increase in the charge transfer resistance after antibody immobilization

The trend shows that upon the modification with anti-nodularin the, the Warburg impedance decreased (Fig. 18), as the immobilised antibody introduces or amplifies the charge transfer resistance (Fig. 19), which is a typical behaviour for the impedance of

antibodies. This therefore shows that the process for the complete immunosensor due to the presence of both the antibody and the quantum dots is a mixed diffusion-kinetic control. Therefore, the equivalent circuit that better describes the electrochemical behaviour of the immunosensor is circuit C, shown in Fig.17.

The bode plots in Fig.20, also show that the phase angle (theta) in table 5, increases upon immobilisation of antibody further confirming that the impedance is moving away from being diffusion controlled (Warburg impedance with an theoretic value of 45 degrees) to a kinetic or mixed diffusion-kinetic controlled process, as observed in the nyquist plots.

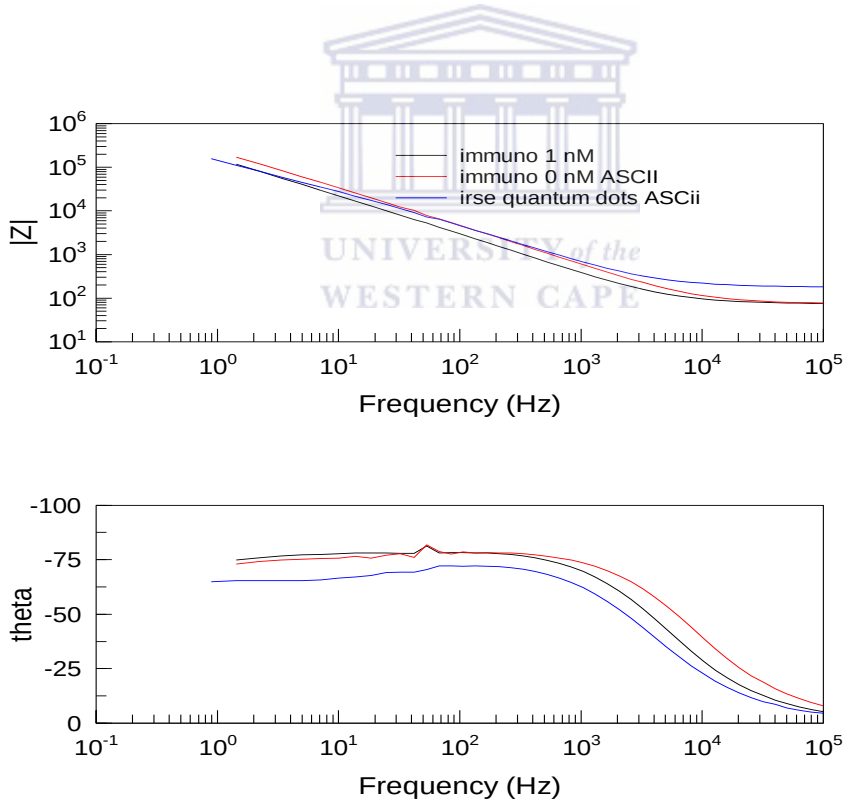

Figure 20 Bode plot for the fabrication process of the 3MPA-$IrSe_2$ quantum dots immunosensor

Table 5 Change in phase angle for electrode systems

Electrode system	Phase angle in degrees
A) 3MPA-$IrSe_2$ quantum dots	64
B) Au/3MPA-$IrSe_2$ qds/antiNodularin	73
C) Au/3MPA-IrSe qds/antiNodularin+1 nM	75

4.3 Immunosensor measurements

The detection of nodularin was performed using electrochemical impedance spectroscopy. Upon successive additions of nodularin from 0-0.1 nM and 0.1-1 nM concentration ranges, the Rct decreased linearly as shown in Fig.21-22.

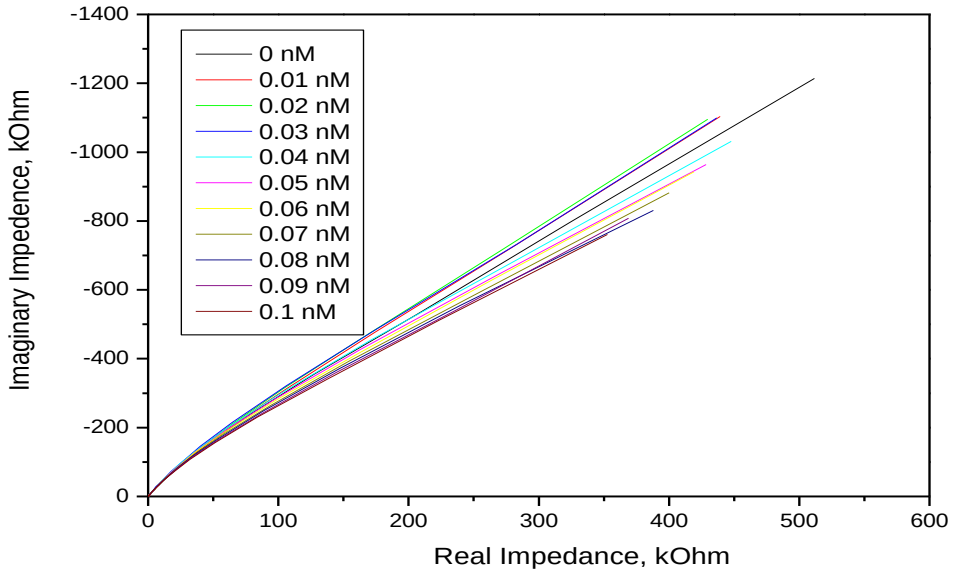

Figure 21 Nyquist plot for the detection of 0.01 -0.1 nM Nodularin, in PBS buffer pH 7.417

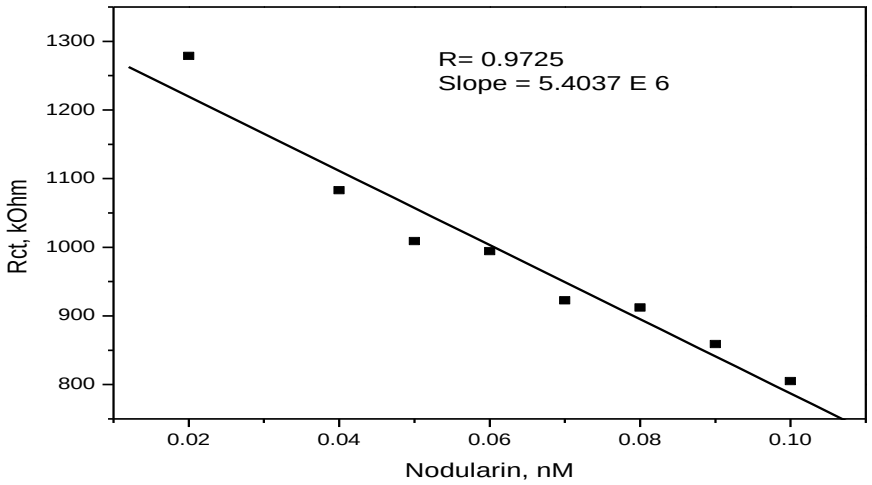

Figure 22 Rct vs Nodularin concentration for successive additions (0.01 to 0.1 nM)

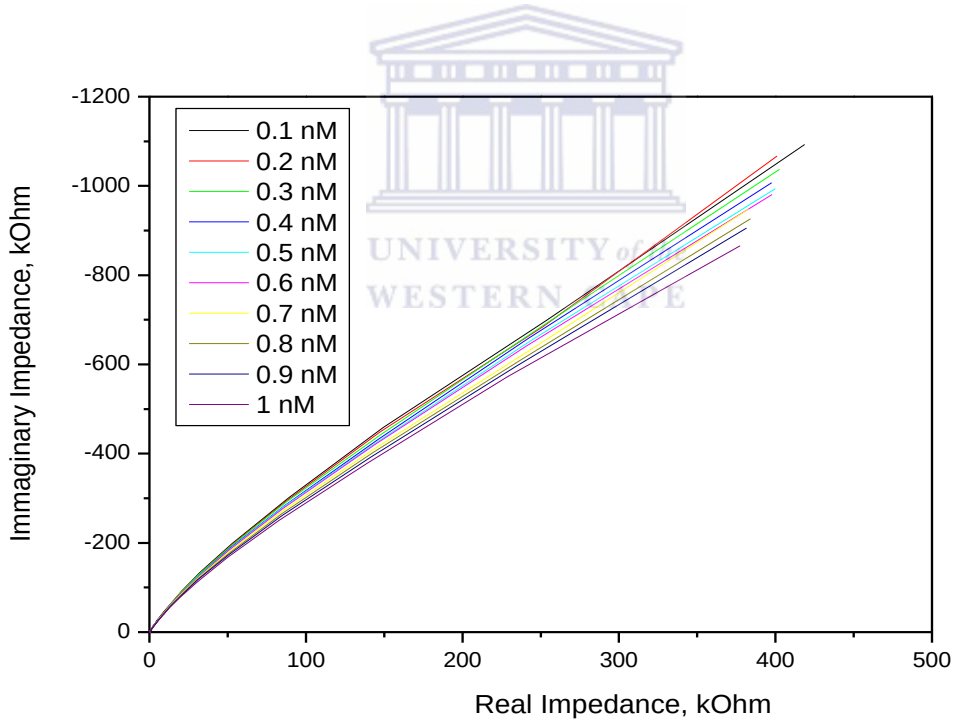

Figure 23 Nyquist plot for the detection of 0.1 -1 nM Nodularin, in PBS buffer pH 7.41

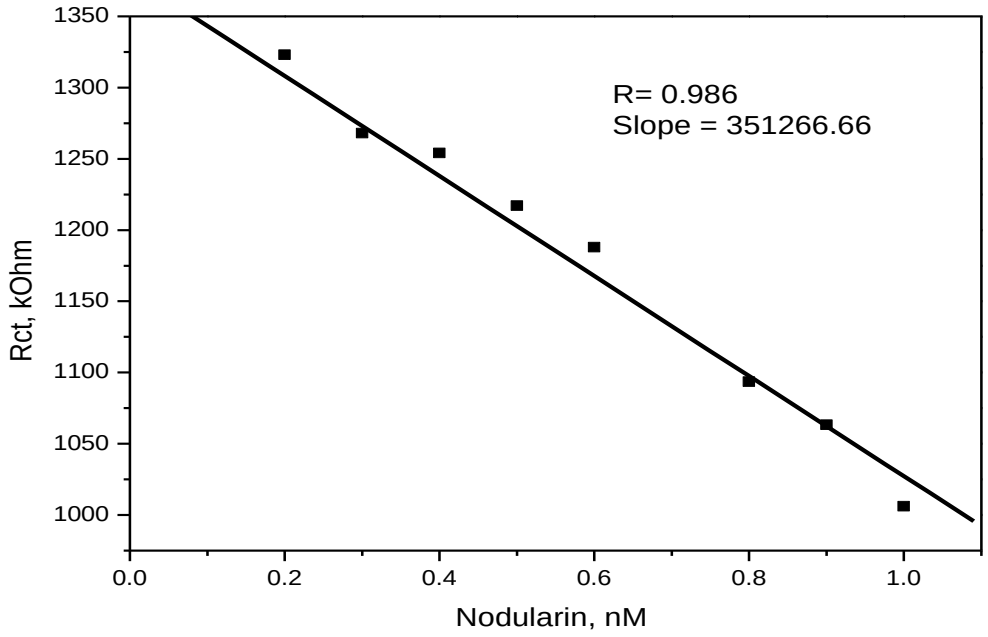

Figure 24 Rct vs Nodularin concentration for successive additions of nodularin (0.1 to 1.0 nM)

The 3MPA-$IrSe_2$ quantum dots based immunosensor was able to detect and distinguish at low nodularin concentrations, ranging between of 0.01 -1 nM as shown in Fig. 22 and Fig.24. The sensitivities of the immunosensor in both concentration ranges are summarized in table 6:

Table 6 Sensitivity and limit of detrection of the immunosensor

Concentration range	Sensitivity in Ohm/ nM	Detection limit	Detection limit in ng/ m L
0.01 nM to 0.1 nM	5.4×10^6 Ω/nM	0.02 nM	0.016 ng/mL
0.1 nM to 1.0 nM	3.5×10^5 Ω/nM	0.011 nM	0.009 ng/mL

The sensitivities are derived from the slope of Fig. 22 and 24 and the detection limits (LOD) is given by:

$$LOD = 3 \times SD \text{ of blank } (\Omega) / \text{Sensitivity } (\Omega/nM) \quad (VI)$$

Where the SD is the standard deviation and SD of Blank measurements is the Rct response of the immunosensor for 8 measurements. The 3MPA-$IrSe_2$ immunosensor constructed in this work, is highly sensitive towards Nodularin, with a detection limit as low as 0.009 ng/mL (n=8, SD=12249.4); which is significantly lower than the recent anti-Nodularin ELISA kit developed by (Zhou et al ., 2011) which has a detection limit of 0.16 ng/mL . This high sensitivity further confirms the electrocatalytic properties of the 3MPA-$IrSe_2$ quantum dots present in the immunosensor.

4B.1 Calibration curve of Au/L-cys/3MPA-GaSe/CYP3A4 biosensor for the detection of 17alpha-ethinylestradiol (17EE).

The detection of 17 EE was performed as described in Nxusani et al., 2012, but now using lower concentration ranges, 0.001-0.1 nM. As shown in Fig.27, the concentration dependant current response has a calibration curve (r^2 = 0.99) with a characteristic plateu of enzymatic reactions. This shows that the biosensor response followed the Michealis-Menten kinetics for enzyme based biosensors (Ndangili et al., 2011).

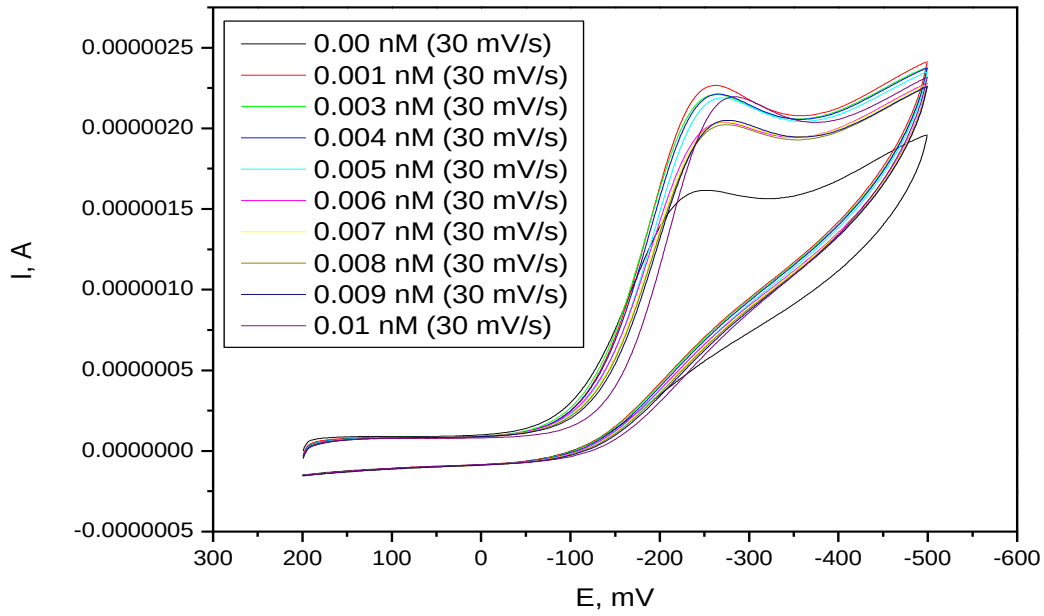

Figure 25 CV response of Au/L-cys/3MPA-GaSe/CYP3A4 Biosensor upon addition of 0.00 -0.01 nM 17 EE at 30 mV/s, in PBS pH7.4

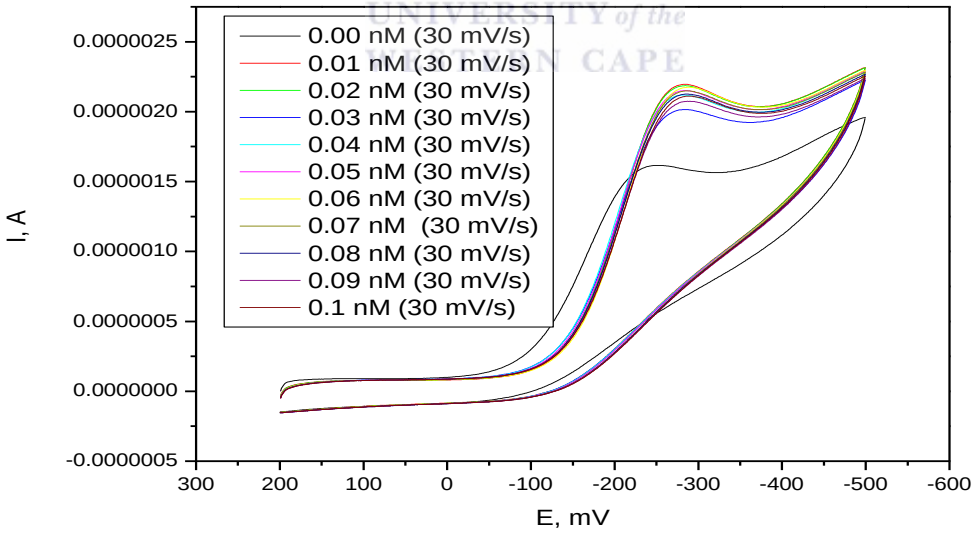

Figure 26 CV response of Au/L-cys/3MPA-GaSe Biosensor upon addition of 0.00 -0.1 nM 17 EE at 30 mV/s, in PBS pH7.4

The sensitivity and detection limit (n = 6, SD = 3.364 x10^{-8}) of the biosensor shown in table 7, is derived from the linear region of the of the biosensor current response (Fig.28), with a linear regression of 0.985.

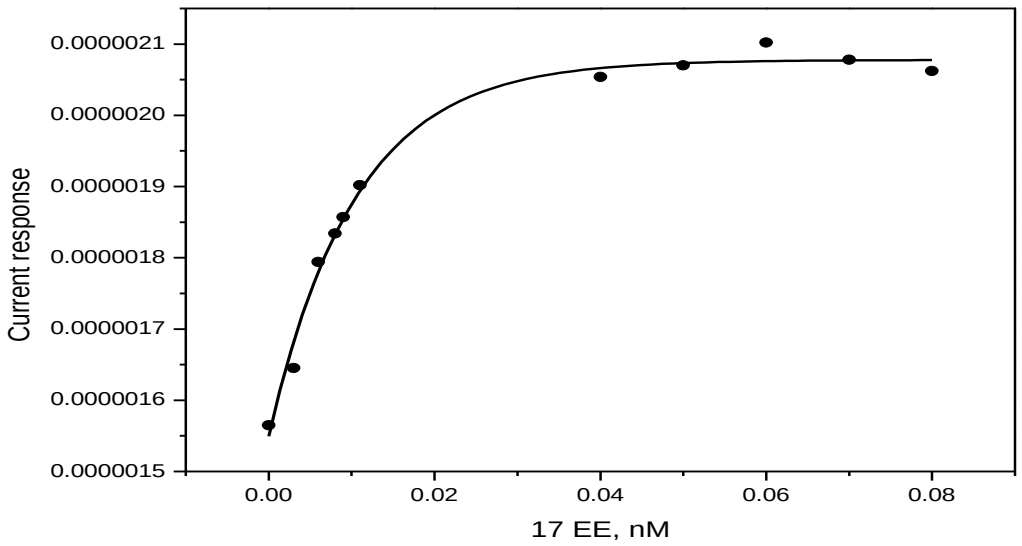

Figure 27 Biosensor response upon successive additions of 17 EE, following a Michaelis-Menten kinetics trend

The Michaelis-Menten constant, K_M^{app}, is a characteristic parameter for the enzyme-substrate kinetics. From the following equation:

$$i = i_{max} [17EE] / K_M^{app} + [17EE] \quad \text{(VII)}$$

where i_{max} is the maximum current measured under saturated substrate concentration and [17EE] is the bulk concentration. K_M^{app} was found to be 0.0073 nM, and the i_{max} was 0.514 µA.

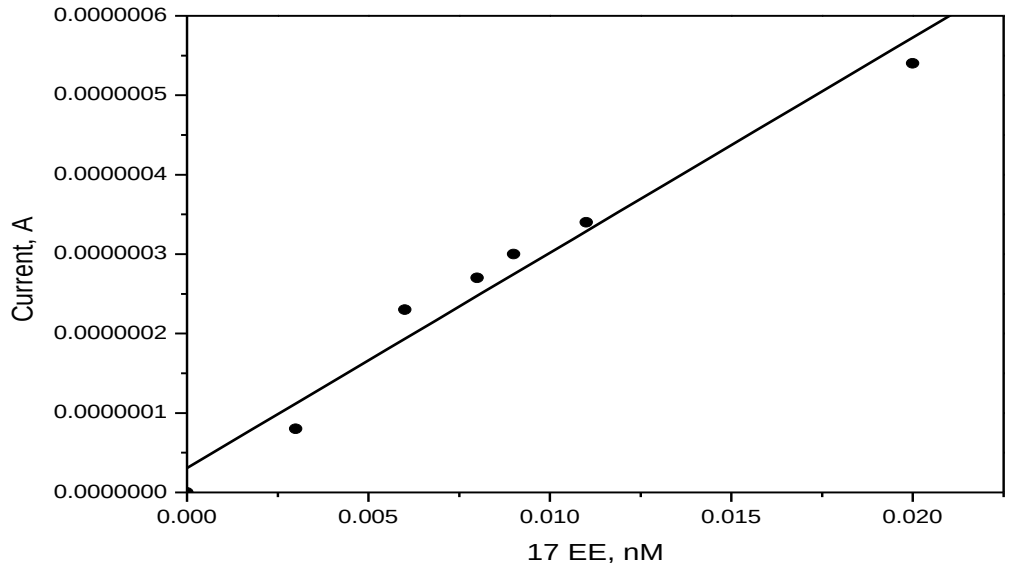

Figure 28 Calibration curve from linear region of the Biosensor response, in Fig. 27

Table 7 Sensitivity and detection limit of the biosensor

Biosensor	Sensitivity in A/ nM	Detection limit	Detection limit in ng/ m L
Au/L-cys/3MPA-Ga_2Se_3 Biosensor	2.709 x 10^{-5} A/ nM	0.004 nM	0.0011 ng/ mL

In this work, Au/L-cys/3MPA-GaSe/ CYP3A4 Biosensor has shown a high sensitivity towards detecting 17EE, with a detection limit as low as 0.0011 ng/mL.

Chapter five

5.0 Conclusion

3 nm 3MPA-$IrSe_2$ quantum dots where successfully synthesised and found to have interesting electro-catalytical properties, with a very low characteristic reduction potential of 107 mV, indicative of a low energy requiring electrochemical process. These were in turn used for the fabrication of the immunosensor towards the detection of Nodularin. The label free impedimetric immunosensor constructed was sensitive towards nodularin, with a very low detection limit of 0.009 ng/mL; which is significantly lower than a recent anti-Nodularin ELISA kit (*Zhou et al., 2011*) which has a detection limit of 0.16 ng/mL. Also the detection limit of the immunosensor is below the maximum South African guideline value for microcystin-LR (0-0.8) µg/L in water (*DWAF; 1996*). Though the surface concentration of the adsorbed 3MPA-$IrSe_2$ on gold electrode is as low as 5.15 x 10^{-13} $mol.cm^{-2}$; the sensitivity of the immunosensor is significantly high, further confirming the excellent electrocatalytic activity of the 3MPA-$IrSe_2$ quantum dots formed.

The calibration curve of the 3MPA-GaSe nanocrystal based biosensor was successfully constructed, which exhibited a trend described by Michaelis-Menten, which is a typical behaviour of enzymatic biosensors. The detection limit of the biosensor is 0.004 nM, which is lower than the action limit of 17beta-estradiol, 1.47 x 10^{-10} M (*Volpe et al., 2006*).

References

1. Y. Zhou., et al, *Detection of nodularin based on a monoclonal antibody in water and aquatic fish samples*. Food Control, **2011**, 22: pp 797-800

2. K.L. Rinehart., et al, *Nodularin, microcystin and the configuration of adda*. Journal of American Chemical Society, **1988**, 110(25): pp 8557-8558

3. S. Yoshizawa., et al, *Inhibition of protein phosphatises by microcystins and nodularin associated with hepatotoxicity*. Journal Cancer Res. Clinical Oncology, **1990**, pp 119:609-14

4. K.E. Fladmark., et al, *Sensitive detection of apoptogenic toxins in suspension cultures of rat and salmon hepatocytes*. Toxicon, **1998**, 36: pp 1101 -14

5. I.R. Falconer., et al, *Health risk assessment of cyanobacterial (blue-green algal) toxins in drinking water.* International journal of environmental research and public health, **2005**, 2

6. N. Bouaicha., et al, *Genotoxic potential of microcystin-LR and nodularin in vitro in primary cultured rat hepatocytes and in viv in rat liver*. Enviromental toxicology, **2005**,20(3): pp 341-7

7. A. Lankoff., et al, *Nodularin induced genotoxicity following oxidative DNA damage and aneuploidy in HepG2 cells*. Toxicology letters, **2006** 164: pp 239-248

8. B.W. Ibelings., et al., *Accumulation of cyanobacterial toxins in freshwater "seafood" and its consequences for public health: a review article*. Environmmental pollution, **2007**, 150: pp 177-192

9. M.F.O.Azevedo., et al., *Human intoxication by microcystins during renal dialysis treatment in Caruaru-Brazil*. Toxixology, **2002**, 182: pp 441-446

10. N Sapeika., et al., *Mussel Poisoning: a recent outbreak. S.A. Medical Journal*, **1958** 527

11. T.A.M. Msagati,, et al., *Evaluation of methods for isolation, detection and quantification of cyanobacterial hepatotoxins: A review article*. Aquatic toxicology, 78 **2006**: pp 382-397

12. WHO, *Report of the working group on chemical substances in drinking water, Section 5.2, microcystin-LR*. World health Organization, Geneva, 22-26 April **1997**. pp1

13. I.R. Falconer., et al., *Safe levels and safe practices*. Toxic cyanobacteria in water, E and FN Spon, London,**1999**: pp 155-178

14. G.A. Codd., et al, *Initial situation assessment and recommendations*. CYANONET, UNESCO IHP-VI, **2005**

15. Department of water affairs and forestry (DWAF), *South African water quality guidelines*. Second edition, Volume 1: Domestic use. **1996**

16. Z.A Peng., et al, *Mechanisms of the shape evolution of CdSe nanocrystals*. Journal of the American chemical society, **2011**, 123(7): pp 1389-1395

17. K. Ueno., et al, *Epitaxial growth of a vacancy-ordered Ga2Se3 thin film on vicinal Si substrate.* Journal of crystal growth, **2002**,237-239: pp 1610-1614

18. J. Park., et al, *Chemical vapour deposition of indium selenide and gallium selenide thin films from mixed alkyl dialkylselenophosphorylamides*. Chemistry of materials, **2003**, 15(22): pp 4205 -4210

19. M. Lazell., et al, *Single source molecular precursor for the deposition of III/VI chalcogenide semiconductors by MOCVD and related techniques*. Journal of the chemical society, **2000**,24: pp 4479-4486

20. A. Markl., et al, *Investigation of Se capping of epitaxial Ga_2Se_3 layers*. Surface science, **1995**, 331-333 : pp 631-635

21. M.A. Afifi., et al, *Determination and analysis of optical constants for Ga2Se3 films near absorption edge*. Physica B: Condensed Matter, **2003**, 325: pp 308-318

22. M. Rusu., et al, *Deposition and characterization of Ga_2Se_3 thin films prepared by a novel chemical close-spaced vapour transport technique*. Journal of Physics: Condensed Matter, **2003**, 15: pp 8185-8194

23. C. Burda., et al, *Chemistry and properties of nanocrystals of different shapes. Chemical Reviews*, **2005**, 105: pp 1025-1102

24. L. Brus., et al, *Electronic wave functions in semiconductor clusters: experiment and theory*. Journal of Physical Chemistry, **1986**, 90 : pp 2555-2560

25. K. Sattler., et al, *The energy gap of nanoparticles, and quantum dots*. Handbook of thin films materials: Nanomaterials and magnetic thin films, **2002**, 5: pp 61-83

26. J. Hambrock., et al, *Synthesis of CdSe nanoparticles using various organometallic cadium precursor*. Journal of materials chemistry, **2001**,11: pp 3197-3201

27. S. Dey., et al., *Platinum Group Metals Chalcogenides: Their synthesis and applications in catalysis and materials science*. Platinum Metals Review, **2004**, 48: pp 16-29

28. Bond, G.C., et al., *Periodic variations in the catalytic properties of metals*. Platinum metals review, **1968**, 12: pp 100-105.

29. B.H. Lipshutz., et al, *Catalysis in the service of green chemistry: Nobel prize-winning palladiuim-catalysed cross-couplings, run in water at room temperature*. Platinum Metals Review, **2012** , 56: pp 62-74

30 W.Liu., et al, *Nanoparticles and their biological and environmental applications*. Journal of Bioscience and bioengineering, **2006**, 102: pp 1-7

31. J.Akhtar., et al, *A novel single source precursor: [bis(N,N-diethyl-N'- naphthoyl-selenoureato)palladium(II)] for palladium selenide thin films and nanoparticles*. The royal society of chemistry: Chem.Comm, **2010.**

32. H. Takahashi., et al, *Preparation of well-crystallized Pd20Te7 alloy nanoparticulate catalysts with uniform structure and composition in liquid-phase*. Applied Catalysis A :General, **2011**,392: pp 80-85

33.P.Singh.,etal,*Palladium(II)complexesof N-{2-(aryltelluro)ethyl}morpholine/piperidine: Synthesis, structure, application in Heck coupling and unprecedented conversion into nano-sized PdTe*. Inorganic Chemistry Communications, **2012**,15: pp 163-166

34. M.M. Almazo., et al, *Synthesis and characterization of rhodium nanoparticles using HRTEM techniques*. Microchemical Journal, **2005**,81: pp 133-138

34. J. R. Lloyd., et al, *Biotechnological synthesis of functional nanomaterials*. Current Opinion in biotechnology: Nanobiotechnology and systems biology, **2011**, 22: pp 509-515

35. A.D.S. Roberts., et al, *Quantum dot infrared photodetectors.* Comprehensive semiconductor science and technology, **2011**, pp 452-485

36. X, Jiang., et al, *Template-engaged synthesis of RuSe and PdSe nanotubes by reacting precursor salts with selenium nanowires*. Chemical Physics letters, **2004**, 385 : pp 472-476

37. A.K. Samal., et al, *Pt_3Te_4 nanoparticles from tellurium nanowires*. Langmuir,**2010**,26 : pp 19136-19141

38. G. Liu., et al , *Facile synthesis of carbon-supported IrxSey chalcogenide nanoparticles and their electrocatalytic activity for the oxygen reduction reaction*. Journal of Physical Chemistry, **2008**, 112 pp 2058-2065

39. J. Cookson., et al, *The preparation of palladium nanoparticles: Controlled sizes are key to producing more effective materials.* Platinum Metals Review, **2012**, 56 : pp 83-89

40. E. Boubour., et al, *Insulating properties of self-assembled monolayers monitored by impedance spectroscopy.* Langmuir, **2000**, 16: pp 4222-4228

41. P.E. Laibinis., et al, *Structure of monolayers formed by co-adsoption of two n-alkanethiols of different chain lengths on gold and its relation to wetting*. Journal of American Chemical Society, 1992, 114 pp:1990

42. R. Haag., et al, *Electrical breakdown of aliphatic and aromatic self-assembled monolayers used as nanometer-thick organic dielectrics*. Journal of American Chemical Society, **1999**,121: pp 7895-7906

43. P.M. Ndangili., et al, *3-Mercaptopropionic acid capped ZnSe quantum dot-cytochrome P450 3A4 enzyme biotransducer for 17beta-estradiol*. Journal of Electroanalytical Chemistry, **2011**, 653: pp 67-74

44. O. Chailapakul., et al, *Synthesis and characterization of simple self-assembling, nanoporous monolayer assemblies: A new strategy for molecular recognition.* Langmuir, **1993**, 9, pp 884 -888

45. S. Moeno., et al, *The determination of the photosensitizing properties of mercapto substituted phthalocyanine derivatives in the presence of quantum dots capped with mercaptopropionic acid*. Journal of photochemistry and photobiologyy A: Chemistry, **2011**, 218 : pp 101-110

46. P. M.Ndangili., et al, *A potential masking approach in the detection of dopamine on 3-mercaptopropionic acid capped ZnSe quantum dots modified gold electrode in the presence of interferences.* Journal of Electroanalytical Chemistry, **2010**, 643: pp 77-81

47. M. Liu., et al, *Quantum dots modified electrode and its application in electroanalysis of haemoglobin*. Electrochemistry Communications, **2006**, 8: pp 305-310

48. J. Idana., et al, Photochemical instability of CdSe nanocrystals coated by hydrophilic thiols. Journal of the American chemical society, 2001, 123: pp 8844-8850.

49. M.J. Giz., et al, *In situ STM study of self-assembled mercaptopropionic acid monolayers for electrochemical detection of dopamine*. Journal of Electroanalytical Chemistry, **1999**,465: pp 72-79

50. J. Li., et al, *Electrochemistry of thiol-capped CdTe quantum dots and its sensing application*. Journal of Electroanalytical Chemistry, **2009**, 625: pp 88-91

51. I.E.J. Barnhoorn., et al, *Histological evidence of intersex in feral sharptooth catfish (Clarias gariepinus) from an estrogen-polluted water source in gauteng, South Africa*. Environmental Toxicology, **2004**,19 : pp 603-608

52. O.O. Olujimi., et al, *Endocrine disrupting chemicals (phenol and phthalates) in the South African environment: a need for more monitering*. Water SA, **2010** 36(5): pp 671-682

53. J.R. Grindley., et al., *The cause of mussel poisoning in South Africa.* S.A Medical Journal, **1969**, 275

54. *European Union Commission Regulation*, EC 2074/2005. Official Journal of the European Union L, **2005**, 338: pp 27–59.

55. *European Union Commission Regulation*, EC 1664/2006. Official Journal of the European Union L, **2006**, 320: pp 13–45.

56. J.E. Gourd., et al, *Metal prices and the cost of pgm chemicals*. Platinum Metals Review, **2004**,48: pp 15

57. W. Joseph.,et al , *Electrochemical biosensors: Towards point-of-care cancer diagnostics.* Biosensors and Bioelectronics, **2006**. 21(10): pp 1887-1892.

58. G. –C. Zhao., et al, *A label-free electrochemical RNA aptamer for selective detection of theophylline.* Electrochemistry Communications, **2010**. 12(2): pp 300-302.

59. T.G. Drummond., et al, *Electrochemical DNA sensors.* Nat Biotech, **2003**. 21(10): pp 1192-1199.

60. K.J. Cash., et al, *Nanosensors and nanomaterials for monitoring glucose in diabetes*. Trends in Molecular Medicine, **2010**,16: pp 584-593

61. N.Bistolas., et al., *Cytochrome P450 biosensors—a review*. Biosensors and Bioelectronics, **2005**. 20(12): pp 2408-2423.

62. A.P. Li., et al, *Substrates of human hepatic cytochrome P450 3A4.* Toxicology, **1995**. 104(1-3): pp 1-8.

63. M.T. Donato., et al, *Strategies and Molecular Probes to Investigate the Role of Cytochrome P450 in Drug Metabolism: Focus On In Vitro Studies.* Clinical Pharmacokinetics, **2003**. 42(2): pp 153-178.

64. V.V. Shumyantseva., et al, *Electrochemical reduction of cytochrome P450 as an approach to the construction of biosensors and bioreactors.* Journal of Inorganic Biochemistry, **2005**. 99(5): pp 1051-1063.

65. N.R. Hendricks., et al, *Microsomal cytochrome P450-3A4 (CYP3A4) nanobiosensor for the determination of 2,4-dichlorophenol- an endocrine disruptor compound*. Electrochimica Acta, **2009**,54: pp 1925-1931

66. C.A. Wijayawardhana., et al, *Milestones of electrochemical immunoassay at Cincinnati*. Electroanalytical methods for biological materials (eds. Braijter-Toth, Chambers) Marcel Dekker, **2002**, pp 329-365

67. E.M. Abad-Villar., et al, *Gold bands as a suitable surface for enzyme immunoassays*. Biosensors and bioelectronics, **2002**, 17: pp 797-802

68. Y. Gong-Jun., et al, *A re-usable capacitive immunosensor for detection of salmonellaspp. Based on grafted ethylene diamine and self-assembled gold nanoparticles monolayer*. Analytica Chimica Acta, **2009**, 647: pp 159-166

69. D. Li, et al, *Label- free capacitative immunosensor based on quartz crystal Au electrode for rapid and sensitive detection of Escherichia coli O157:H7*. Analytica Chimica Acta, **2011**, 687: pp 89-96

70. Y. Li., et al, *Amperometric immunosensor for the detection of Escherichia coli O157:H7 in food specimens*. Analytical Biochemistry, **2012**, 1: pp 227-33

71. S. Dawan., et al, *Label-free capacitive immunosensors for ultra-trace detection based on the increase of immobilized antibodies on silver nanoparticles*. Analytica Chimica Acta, **2011**, 699: pp 232-241

72. G. Liu., et al, *Towards the fabrication of label-free amperometric immunosensors using SWNTs*. Electrochemistry communication, **2009**, 11: pp 1982-1985

73. L. Zhang., et al, *Attachment of gold nanoparticles to glassy carbon electrode and its application for the direct electrochemistry and electrocatalytic behaviour of haemoglobin.* Biosensors and Bioelectronics, **2005**, 21 : pp 337-345

74. M.J.N. Pourbaix., et al, *Electrochemical properties of the platinum metals*. Platinum review metals, **1959**, 3 (3): pp 100 - 106

75. J. Drbohlavova., et al.,*Quantum Dots — Characterization, Preparation and Usage in Biological Systems.* International Journal of Molecular Sciences, **2009**. 10(2): pp 656-673.

76. L. de Alda., et al, *Determination of steroid sex hormones and related synthetic compounds considered as endocrine disrupters in water by liquid chromatography–diode array detection–mass spectrometry.* Journal of Chromatography A, **2000**, 892(1-2): pp 391-406

77. J.A. Russell., et al, *High-performance liquid chromatographic determination of 17β-estradiol and 17β-estradiol-3-acetate solubilities and diffusion coefficients in silicone elastomeric intravaginal rings.* Journal of Chromatography B: Biomedical Sciences and Applications, **2000**, 744(1): pp 157-163

78. Y. Yoon., et al, *HPLC-fluorescence detection and adsorption of bisphenol A, 17β-estradiol, and 17α-ethynylestradiol on powdered activated carbon.* Water Research, **2003**. 37(14): pp 3530-3537.

79. Mishra., et al,*HPLC-electrochemical detection of ovarian estradiol-17β and catecholestrogens in the catfish Heteropneustes fossilis: Seasonal and periovulatory changes.* General and Comparative Endocrinology, **2006**. 145(1): pp 84-91.

80. L. Zhao., et al., *Development of a highly sensitive, second antibody format chemiluminescence enzyme immunoassay for the determination of 17β-estradiol in wastewater.* Analytica Chimica Acta, **2006**. 558(1-2): pp 290-295.

81. H.-B. Wei., et al., *Detection of 17β-Estradiol in River Water and Human Urine by Highly Sensitive Chemiluminescence Enzyme Immunoassay.* Chinese Journal of Analytical Chemistry, **2007**. 35(3): pp 319-324.

82. G. Volpe., et al., *A disposable immunosensor for detection of 17β-estradiol in non-extracted bovine serum.* Analytica Chimica Acta, **2006**. 572(1): pp 11-16.

83. Y.S Kim., et al., *Electrochemical detection of 17β-estradiol using DNA aptamer immobilized gold electrode chip.* Biosensors and Bioelectronics, **2007**. 22(11): pp 2525-2531.

84. J. Song., et al, *Electrochemical determination of estradiol using a polyfilm-modified electrode.* Journal of Applied Electrochemistry, **2008**. 38(6): pp 833-836.

85. N. Terui., et al, *Voltammetric Behaviour and Determination of 17b-Estradiol at Multi-Wall Carbon Nanotube-Nafion Modified Glassy Carbon Electrode.* Analytical Sciences, **2006**. 22: pp 895-898.

86. T.M. Crisp., et al., *Environmental Endocrine Disruption: An Effects Assessment and Analysis.* Environmental Health Perspectives,the National Institute of Environmental Health Sciences (NIEHS),**1998**, 106: pp 11-56.

87. K. Lah., et al, *National Institute of Environmental Health Sciences (NIEHS), Endocrine Disruptors.*

2011.

88. R. Céspedes., et al., *Distribution of endocrine disruptors in the Llobregat River basin (Catalonia, NE Spain).* Chemosphere, **2005**, 61(11): pp 1710-1719.

89. R. Kase., et al., *Integral assessment of estrogenic potentials of sediment-associated samples.* Environmental Science and Pollution Research, **2008**, 15(1): pp 75-83.

90. F. Lahnsteiner., et al., *Effect of 17β-estradiol on gamete quality and maturation in two salmonid species.* Aquatic Toxicology, **2006**. 79(2): pp 124-131.

91. H. Segner., et al., *Identification of endocrine-disrupting effects in aquatic vertebrates and invertebrates: report from the European IDEA project.* Ecotoxicology and Environmental Safety, **2003**. 54(3): pp 302-314.

92. S. Jobling., et al, *Comparative responses of molluscs and fish to environmental estrogens and an estrogenic effluent.* Aquatic Toxicology, **2003**. 65(2): pp 205-220

93. B. Campbell., et al, *Endocrine Changes During Onset of Puberty in Male Spring Chinook Salmon, Oncorhynchus tshawytscha.* Biology of Reproduction, **2003**. 69(6): pp 2109-2117.

94. T. Miura., et al, *Molecular control mechanisms of fish spermatogenesis.* Fish Physiology and Biochemistry, **2003**. 28(1): pp 181-186.

95. R..E.Peter., et al, *Neuroendocrine regulation of ovulation in fishes: basic and applied aspects* Reviews in Fish Biology and Fisheries, **1997**. 7: p. 173-197.

96. D.E Kime.,et al, *Classical' and 'non-classical' reproductive steroids in fish.* Reviews in Fish Biology and Fisheries **1993**. 3: pp 160-180.

97. L.S. Shore., et al, *Naturally produced steroid hormones and their release into the environment.* Pure and Applied Chemistry, **2003**. 75.: pp 1859-1871.

98. C.G. Campbell., et al., *Biologically directed environmental monitoring, fate, and transport of estrogenic endocrine disrupting compounds in water: A review.* Chemosphere, **2006**. 65(8): pp 1265-1280.

99. O. Braga., et al, *Steroid estrogens in ocean sediments.* Chemosphere, **2005**. 61(6): pp 827-833.

100. Y . Tamagawa., et al., *Removal of estrogenic activity of natural steroidal hormone estrone by ligninolytic enzymes from white rot fungi.* Chemosphere, **2006**. 65(1): pp 97-101.

101. D.G.J Larsson., et al., *More male fish embryos near a pulp mill.* Environmental Toxicology and Chemistry, **2000**. 19(12): pp 2911-2917.

102. Y. Oshima., et al., *Suppression of sexual behaviour in male Japanese medaka (Oryzias latipes) exposed to 17β-estradiol.* Chemosphere, **2003**. 50(3): pp 429-436.

103. M. Teles., et al., *Juvenile sea bass biotransformation, genotoxic and endocrine responses to β-naphthoflavone, 4-nonylphenol and 17β-estradiol individual and combined exposures.* Chemosphere, **2004**. 57(2): pp 147-158.

104. N. Lehtimaki., et al, *Nodularin uptake and induction of oxidative stress in spinach (Spinachia oleracea).* Journal of Plant Physiology, **2011**, 168: pp 594-600

105. E. Nxusani., et al, *3-mercaptopropionic acid capped Ga_2Se_3 nanocrystals-cyp3a4 biosensor for the determination of 17alpha-ethinylestradiol in water*. NanoHybrids, **2012**, 1: pp 1-22

106. P.N. Ndangili., et al, *Impedimetric response of a lable free genosensor prepared on 3-mercaptopropionic acid capped gallium selenide nanocrystal modified electrode*. International Journal of electrochemical science, **2011**, 6: pp 1438 – 1453

107. C. Shen., et al, *One-step synthesis of white-light emitting quantum dots at low temperature.* Inorganic chemistry, **2009**, 48: pp 8689 - 8694